

Dynamic vehicle-track interaction and differential settlement in a transition zone on railway ballast-- An integrated 3D discrete-continuum model

Downloaded from: https://research.chalmers.se, 2025-11-09 22:22 UTC

Citation for the original published paper (version of record):

Ahmadi, A., Nasrollahi, K., Nielsen, J. et al (2026). Dynamic vehicle–track interaction and differential settlement in a transition zone on railway ballast-- An integrated 3D discrete–continuum model. Computers and Geotechnics, 190. http://dx.doi.org/10.1016/j.compgeo.2025.107737

N.B. When citing this work, cite the original published paper.

research.chalmers.se offers the possibility of retrieving research publications produced at Chalmers University of Technology. It covers all kind of research output: articles, dissertations, conference papers, reports etc. since 2004. research.chalmers.se is administrated and maintained by Chalmers Library

ELSEVIER

Contents lists available at ScienceDirect

Computers and Geotechnics

journal homepage: www.elsevier.com/locate/compgeo



Research paper

Dynamic vehicle–track interaction and differential settlement in a transition zone on railway ballast—An integrated 3D discrete–continuum model

Alireza Ahmadi a , Kourosh Nasrollahi b , Jens C.O. Nielsen b , Jelke Dijkstra c

- a Department of Civil and Architectural Engineering, Division of Soil and Rock Mechanics, KTH Royal Institute of Technology, SE-100 44, Stockholm, Sweden
- b Department of Mechanics and Maritime Sciences, Division of Dynamics/CHARMEC, Chalmers University of Technology, SE-412 96, Gothenburg, Sweden
- Department of Architecture and Civil Engineering, Division of Geology and Geotechnics, Chalmers University of Technology, SE-412 96, Gothenburg, Sweden

ARTICLE INFO

Keywords: Transition zone Discrete element method Finite element method Coupled model Differential settlement

ABSTRACT

A numerical methodology for simulating the mechanisms during the initial phase of differential settlement in a railway transition zone using an integrated discrete-continuum approach is presented. The methodology involves the coupling of the Discrete Element Method (DEM), the Finite Difference Method (FDM), and the Finite Element Method (FEM) to model the vertical dynamic interaction between vehicle and transition zone. Specifically, the extensive three-dimensional (3D) DEM model captures the discrete granular behaviour of the ballast and sub-ballast layers, while the continuum-based FDM model is employed to represent the rail structure and the subgrade layer. Based on a time-domain representation of vertical dynamic vehicle-track interaction, the nonlinear two-dimensional (2D) FEM model of the track, together with a multi-body system (MBS) model of the vehicle, is used to calculate the contact forces between wheels and rails. These forces are subsequently used as input to the DEM-FDM simulation for evaluating the non-uniform permanent displacements that will evolve within the granular layers. The support stiffness for each sleeper that is used as input in the FEM model is precomputed during the DEM-FDM coupling stage by applying a static load to each sleeper and calculating the resulting displacement. The developed methodology effectively simulates the progressive formation of voids beneath the sleepers, the redistribution of sleeper-ballast contact force between adjacent sleepers, and the evolving irregularity in vertical track alignment due to the accumulated traffic loading. The approach is demonstrated for a transition zone involving a stiffness gradient between a softer track on ballast and a stiffer track form, and accumulated settlements are calculated for a total of 500 axle passages. The proposed hybrid DEM-FDM-FEM framework provides critical insights into track degradation mechanisms, emphasising the importance of designing a gradual variation in track stiffness to mitigate dynamic loading leading to long-term differential track settlement, thereby reducing maintenance requirements in railway transition zones.

1. Introduction

In a transition zone between two distinct track forms, there is a gradient in vertical track stiffness. Typical examples include transitions between different superstructures, such as from slab track to ballasted track, or between different substructures, such as from an embankment to a bridge or tunnel (Zuada Coelho et al., 2011; Paixão et al., 2014; Sañudo et al., 2016; Wang and Markine, 2018; Guo and Zhai, 2018; Aggestam and Nielsen, 2019; Fărăgău et al., 2019; Indraratna et al., 2019; Shan et al., 2020; Seyyedan et al., 2021; Ramos et al., 2022; de Oliveira Barbosa et al., 2022; Chumyen et al., 2023; Punetha and Nimbalkar, 2023; Heydari, 2023; Ognibene, 2023; Nasrollahi et al., 2023; Jain et al., 2025; Stastny et al., 2025; Siahkouhi et al., 2025). Traffic loading and differences in support conditions on either side of

the transition may lead to differential settlement, voided sleepers, and irregularities in longitudinal track level shortly after construction. Fig. 1 presents a schematic view of the degradation process that typically occurs in ballasted railway transitions, illustrating how problems may arise either in the ballast or in the subgrade. It also clarifies the concept of differential settlements in railway tracks, defined as track support permanent displacements that create an uneven longitudinal rail profile. Such irregularities intensify dynamic loading in the transition zone, accelerating the deterioration of ballast and subgrade, and progressively worsening the vertical track geometry (Nasrollahi et al., 2023; Ahmadi and Larsson, 2025). Consequently, track sections adjacent to transition zones commonly experience rapid degradation,

E-mail address: alahmadi@kth.se (A. Ahmadi).

^{*} Corresponding author.

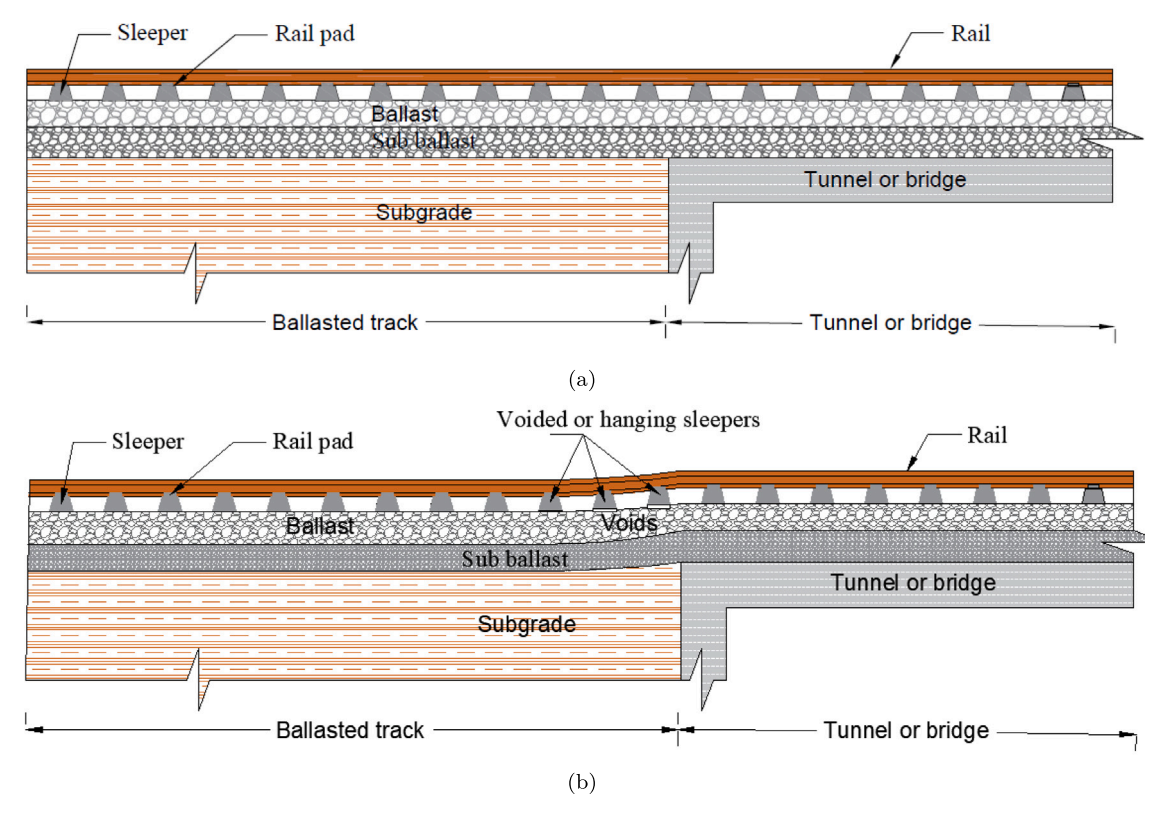


Fig. 1. Schematic representation of track geometry degradation in a transition zone between an open track and a stiffer structure, such as a bridge or tunnel. (a) before any wheel passages, and (b) after multiple wheel passages.

necessitating frequent and costly maintenance to restore track geometry and support conditions (Nasrollahi et al., 2024b).

In railway infrastructure, track settlement and ballast degradation primarily result from particle rearrangement and densification under repeated axle loading. Ballast particles undergo various deterioration mechanisms, including crushing, abrasion (attrition), impact-induced fatigue fracture, surface polishing, freeze—thaw spalling, and chemical weathering, all of which contribute to fines production and ballast fouling (Indraratna et al., 2011; Aela et al., 2024). Concurrently, sleeper rotation, non-uniform load distribution, and stress concentration at transition zones exacerbate localised settlements. Moreover, subgrade deformation mechanisms, such as compaction and consolidation of soil, creep (Zuada Coelho et al., 2021), and plastic deformation in finegrained soils, in conjunction with moisture variations, frost heave, and subsequent thaw-induced settlements, significantly compromise ballast interlocking capacity and shear resistance (Selig and Waters, 1994).

The impact of gradients and abrupt changes in vertical stiffness at the rail level on accumulated track degradation has been extensively investigated through in situ measurements and numerical simulations (see, e.g., Indraratna et al., 2019; Aggestam and Nielsen, 2019; Shan et al., 2020; Nasrollahi et al., 2024b,a). Traditionally, a transition zone design aims to minimise the difference in track stiffness at rail level between the ballasted track and the adjacent engineering structure (Indraratna et al., 2019; Sañudo et al., 2016; Nasrollahi et al., 2024b). Therefore, mitigation measures are employed to achieve a smoother stiffness transition, including under sleeper pads (USPs), transition wedges, approach slabs, auxiliary rails, and varying sleeper configurations on the ballasted side (Sañudo et al., 2016; Indraratna et al., 2019; Fărăgău et al., 2023; Nasrollahi and Nielsen, 2024), as well as varying rail pad stiffness on the slab side (Aggestam and Nielsen, 2019). These techniques help distribute dynamic loads more uniformly across the foundation, thereby reducing the transferred dynamic load to the layers beneath the rail, resulting in a lower risk of accelerated track degradation.

The main challenge in railway transition zones lies in the limited ability to predict the spatial and temporal development of long-term differential settlements. Shifting from reactive to proactive maintenance requires the use of robust and reliable numerical models. Significant research efforts have focused on understanding and predicting long-term settlements in railway transition zones. Generally, two main approaches have been adopted. The first approach utilises a simplified one-dimensional (1D) Winkler-type or 2D discretely supported track model combined with an empirical settlement formula, as presented in Nielsen and Li (2018), Nasrollahi et al. (2023, 2024b). Such empirical models typically rely on cyclic triaxial tests, reducedscale physical experiments, or in situ measurements for calibration. However, track irregularities evolve continuously with each passing axle load resulting in variations in dynamic wheel-rail contact forces, stress distributions within track layers, and settlement. Therefore, without a predictive constitutive model, simulating ballast behaviour with only data from a cyclic triaxial test is insufficient. While empirical models may offer accuracy comparable to constitutive models for the prediction of accumulated settlements, fewer input parameters are typically required (Ramos et al., 2022). In contrast, constitutive models, although capable of capturing complex track behaviour more explicitly, incur significantly higher computational costs (Shan et al., 2020). The second modelling approach involves detailed FEM simulations on continuum scale or a DEM framework to explicitly model local deformations and stresses within the track substructure (Dahlberg, 2001; Suiker and de Borst, 2003; Sun et al., 2014; Vizcarra et al., 2016; Guo and Zhai, 2018). DEM is a powerful tool for analysing granular materials, offering insights into both particle-scale and overall system behaviour.

To capture the complex behaviour of a ballasted railway track, it is essential to model both the discrete nature of the ballast layers and the continuous behaviour of the track superstructure and underlying soil. The DEM is particularly well suited for simulating granular

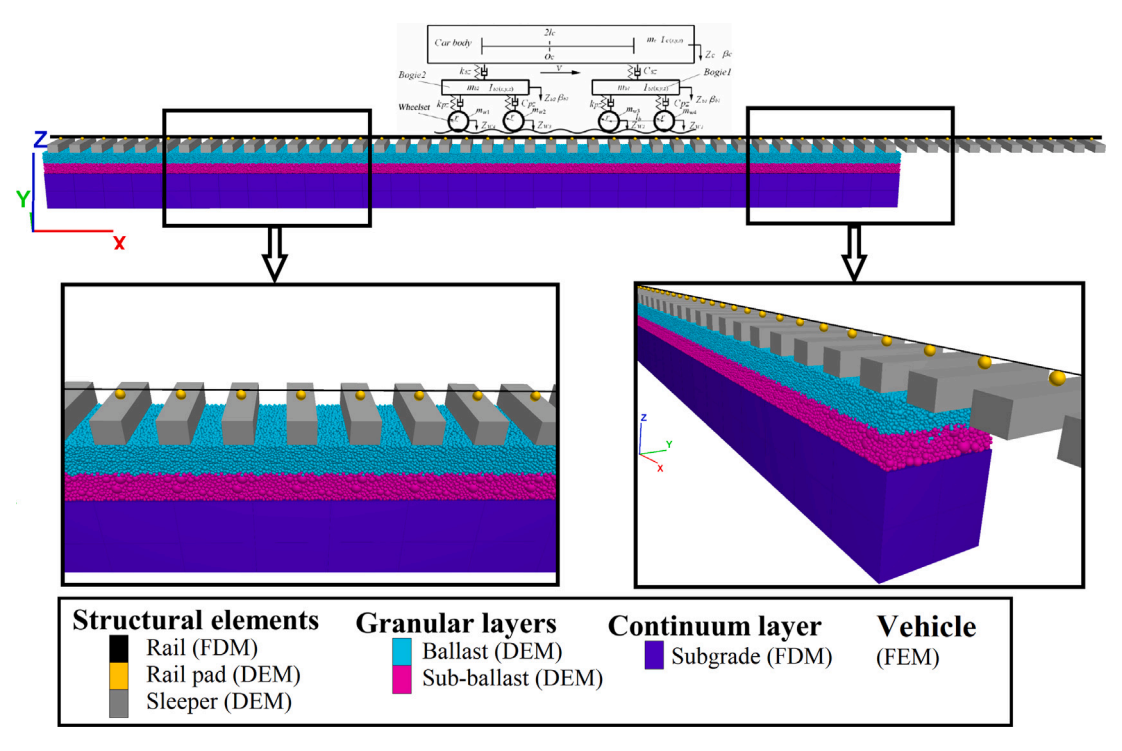


Fig. 2. Integrated DEM-FDM-FEM model.

materials as it enables a direct tracking of particle interactions, rearrangements, breakages, and the effects of particle shape and size variability (Radjai and Dubois, 2011; O'Sullivan, 2011; Nie et al., 2020; Suhr et al., 2022). This level of detail makes DEM superior to traditional continuum-based approaches when it comes to representing the heterogeneous force transmissions and localised deformation typical of coarse-grained granular media. However, the discrete framework of DEM makes it less effective for modelling materials that largely exhibit homogeneous material behaviour at the scale of interest, such as soils in the subgrade, rail and sleepers. These elements are better represented using continuum mechanics approaches. Therefore, a coupled modelling strategy should be adopted, where the ballast is modelled using DEM, while the other materials composed of smaller particles are simulated using a continuum approach, i.e. in this case the Finite Difference Method (FDM). This coupling enables a comprehensive simulation framework that leverages the strengths of both methods, i.e. an accurate particle-scale resolution for the ballast and an efficient continuum representation for the structural layers, thereby providing a more realistic and complete simulation of the dynamic response in a transition to a ballasted track. This approach establishes a direct connection between particle-scale mechanisms and system-scale outcomes. The rearrangement of ballast grains, loss and recovery of sleeper support, and transient re-contact events occur at the scale of individual particles, yet they collectively govern macroscopic quantities such as track stiffness variation, vibration amplitudes, and long-term differential settlement.

This study investigates the initial phase of differential settlement in a ballasted railway transition zone using an integrated DEM-FDM-FEM framework that directly links particle-scale mechanics with system-scale dynamic responses. Unlike conventional empirical, discrete, or purely continuum-based models, the proposed method explicitly simulates the physical mechanisms that drive the evolution of settlement caused by the rearrangements and rotations of ballast and sub-ballast particles under dynamic loading. The ballast and sub-ballast are modelled using the DEM to capture grain-scale rearrangement, contact forces, and void development, while the subgrade and structural elements are represented using the FDM for efficient continuum modelling

of stiffness. Given that in Sweden granite is commonly used for ballast, and that particle rearrangements and rotations are considered the governing mechanisms, the modelling of ballast breakage and particle abrasion has not been explicitly considered. In parallel, a nonlinear FEM-MBS vehicle-track interaction model captures the dynamic amplification of wheel-rail contact forces induced by the abrupt stiffness gradient across the transition zone (differential settlement and an initial misalignment at the rail level can also be considered, which is not the case in many studies). This three-domain model is iteratively coupled, ensuring a two-way interaction between evolving differential settlement and dynamic loading, which has not been achieved in previous studies relying on one-way or simplified coupling strategies. To minimise boundary effects and realistically reproduce the spatial evolution of track behaviour, a long 3D domain of the transition zone is established using a specialised Periodic Replication technique. This allows the model to fully capture 3D stress redistribution, load transfer mechanisms, and lateral confinement effects that cannot be represented in shorter or 2D models. To the authors' knowledge, this constitutes the most extensive and detailed 3D coupled model of a ballasted transition zone developed to date. By integrating discrete element and finite difference modelling, and vehicle-track dynamics in a single computational framework, this approach overcomes key limitations of existing models and provides new insight into the fundamental mechanisms governing differential settlement in railway transition zones.

The paper is structured as follows: Section 2 describes the track and vehicle models used in this paper, and the simulation procedure. Section 3 includes a verification and validation of the models. Section 4 presents numerical examples illustrating the calculated dynamic responses and the initial phase of long-term differential settlement in a transition zone. Finally, Section 5 concludes the paper with a summary and outlook on future work.

2. Methodology

This study develops a numerical and iterative DEM-FDM-FEM framework that captures both the discrete behaviour and evolving settlement of granular layers and the continuum response of the super-structure and subgrade. To accurately represent the dynamic behaviour

Table 1
Summary of methods and key parameters used to represent each vehicle and track component in the integrated DEM-FDM-FEM framework.

Component	Method	Key parameters	Section
Vehicle	MBS	Axle load, speed	2.5
FEM track model	FEM-MBS	Wheel-rail contact force	2.5
Rail	FDM	Young's modulus, density, bending stiffness	2.4
Rail pad	DEM	Rail pad stiffness	2.4
Sleeper	DEM	Mass, bending stiffness	2.4
Ballast	DEM	Particle size, shape, contact stiffness, friction	2.1
Sub-ballast	DEM	Particle size, shape, contact stiffness, friction	2.1
Subgrade	FDM	Young's modulus, density, cohesion, friction	2.3

of the transition zone, the framework incorporates the stiffness gradient between the softer and stiffer track forms, as well as the variation in support stiffness within each track form. The track model combines a 3D DEM model of the ballast and sub-ballast layers with a continuum-based FDM model representing the rail structure and the subgrade layer. In addition, a nonlinear 2D FEM model of the track is coupled with an MBS model of the vehicle. An overview of the complete coupled model is presented in Fig. 2, which illustrates the representation of the rail, rail pads, sleepers, ballast, sub-ballast, and subgrade within their respective domains. Table 1 summarises the applied method and key parameters for each part of the model. Further explanation regarding each part will be given in Section 2.1 to Section 2.5, as listed in the table.

To reduce simulation time, symmetric vehicle and track properties are assumed with respect to the centreline between the two rails in the MBS-FEM and DEM-FDM models. The MBS-FEM model simulates the vertical dynamic interaction between a full vehicle model and the transition zone, generating wheel-rail contact forces that serve as input to the discrete-continuum model. In the MBS model, the vehicle is represented by a carbody and two bogies, each supported by two wheelsets. The discrete model, implemented within a DEM framework, captures the granular nature of the ballast by incorporating irregular particle shapes and realistic size distributions.

Additionally, an FDM approach is employed to represent the components that may be described as continua, such as the rail as a 1D continuous beam and the subgrade beneath the granular layer as a 3D continuum. The FDM approach is selected due to its compatibility with the DEM model, particularly regarding the built-in software integration available for PFC3D-FLAC3D coupling. The built-in PFC3D-FLAC3D coupling, implemented by default and verified in recent research, further ensures efficiency and reliability, whereas alternative methods would have required manual code coupling and additional verification. Methodologically, the concurrent DEM-FDM coupling across the ballast-sub-ballast and rail-subgrade interfaces, combined with a 2D MBS-FEM loop for vehicle-track dynamics, is particularly suited to capturing stiffness gradients, discrete sleepers, and evolving contact gaps. Throughout, adopted strategies such as the Periodic Cell Replication Method, which accelerate the assembly of large DEM ballast domains, also align naturally with this explicit DEM framework but do not map directly to Gauss-point-based DEM integration.

Although the DEM–FDM model operates in three dimensions, some of the degrees of freedom of the structural elements (such as rails, railpads and sleepers) are fixed in one dimension. Only the ballast and sub-ballast particles retain full 3D mobility to accurately simulate their granular behaviour. This controlled dimensionality allows integration with the 2D MBS model for vehicle–track interaction, ensuring consistency between the models without compromising the dynamic representation of the system.

As a result, a comprehensive transition zone model is constructed, consisting of 40 sleepers on the softer side and 10 sleepers on the stiffer side. The softer side of the transition includes the rail, rail pads, sleepers, ballast, sub-ballast, and subgrade.

The overall modelling workflow is summarised in the flowchart shown in Fig. 3. The procedure begins with the generation of representative granular assemblies in the DEM domain and coupling them with

the FDM representation of the subgrade and structural components. In parallel, track and vehicle models are created in the FEM-MBS domain, and static sleeper support stiffness is evaluated in both FEM-MBS and DEM-FDM models. During each iteration, wheel–rail contact forces are calculated in the FEM-MBS domain and transferred to the coupled DEM-FDM track model, where the resulting permanent displacements of the sleeper are calculated and then exported back to update the FEM vehicle–track system. This loop continues until the prescribed number of wheel passages is achieved.

2.1. Discrete element model of granular material

DEM is a numerical technique that is used to simulate the behaviour of granular materials. It is widely applied in geomechanics, particularly in railway engineering, geotechnical engineering and powder technology (Aela et al., 2024). A ballasted railway track comprises both continuous and granular media, including rails, sleepers, fastening systems, ballast, and subgrade. Due to their particulate nature and large grain sizes, ballast and sub-ballast are particularly suitable for DEM modelling, where interactions between individual particles are simulated based on force—displacement laws, and particle motion is updated according to Newton's second law, as originally introduced by Cundall and Strack (1979). In this study, the approach for developing the DEM model and its input parameters is based on the methodology developed by Ahmadi et al. (2024b).

2.1.1. Particle size distribution

The granular structure consists of two layers, each with a thickness of 30 cm, representing the ballast and sub-ballast. The ballast layer comprises coarse, angular particles with diameters ranging from 32 mm to 80 mm, which is shown in Fig. 4, while the sub-ballast layer was assigned a broader particle size distribution, which in reality spans approximately 0.1 mm to 150 mm. However, in the numerical model, the lower cutoff of the sub-ballast particles was increased to 25 mm, resulting in a simulated range of 25 mm to 150 mm. This scaling was implemented to avoid prohibitively small timesteps in explicit DEM, where the critical timestep $\Delta t_{\rm cr} \propto \sqrt{m_{\rm min}/k_n}$ is governed by the smallest particle mass m_{min} and the prescribed contact stiffness k_n . Enlarging the smallest particles, increases m_{\min} and thus enables feasible computation times without compromising the targeted physical processes, such as void formation beneath sleepers, load redistribution, and settlement evolution. The simulation, even with this adjustment, required approximately four months of wall-clock computation time with a CPU 13th Gen Intel(R) Core(TM) i9-13900K. The model contained 259 360 ballast and 112 650 subballast particles. Using actual fine particle sizes (e.g., 0.1 mm instead of the scaled 25 mm) would have increased the runtime by at least 100 times. Such a particle size scaling is a common and well-established practice in multiscale granular modelling to bridge laboratory-scale particle sizes and computationally tractable timesteps. Previous studies have demonstrated that this adjustment does not substantially alter the underlying mechanisms or affect the simulation results (Wang et al., 2022; Ahmadi et al., 2023; Dorador and Villalobos, 2020; Nakamura et al., 2020; Bian et al., 2020; Yousefi and Ng, 2017; Lommen et al., 2019; Guo and Zhao, 2014). The

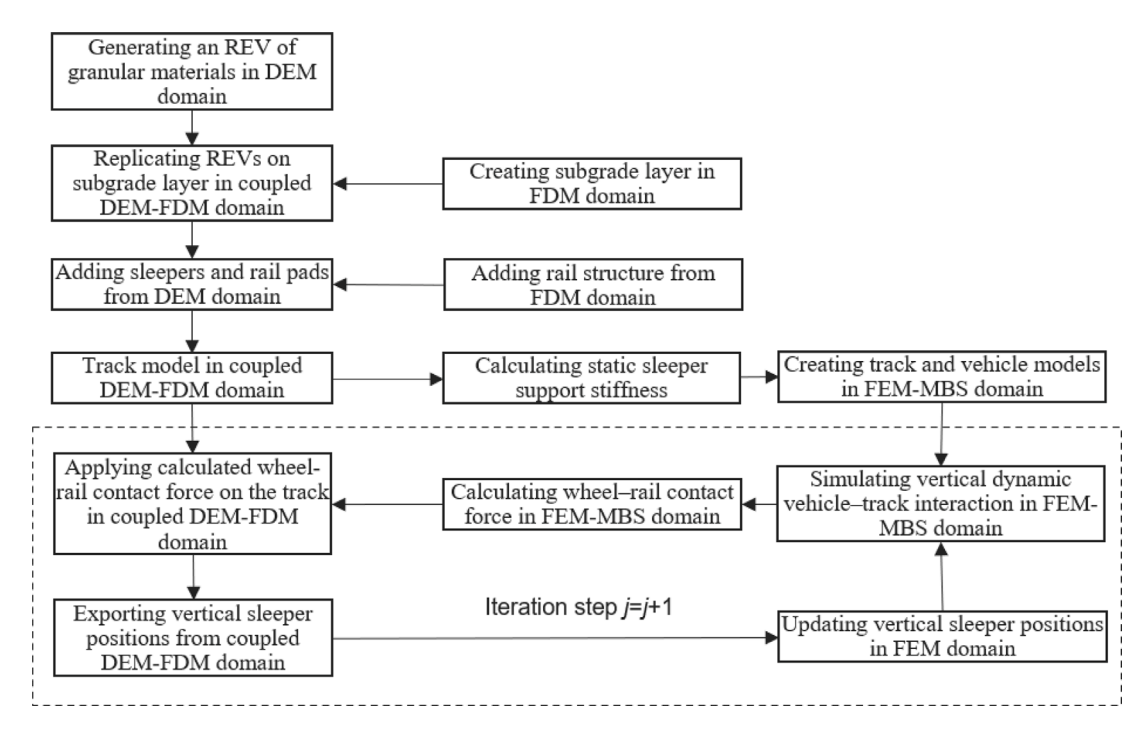


Fig. 3. Flowchart of the different steps in the iterative simulation methodology.

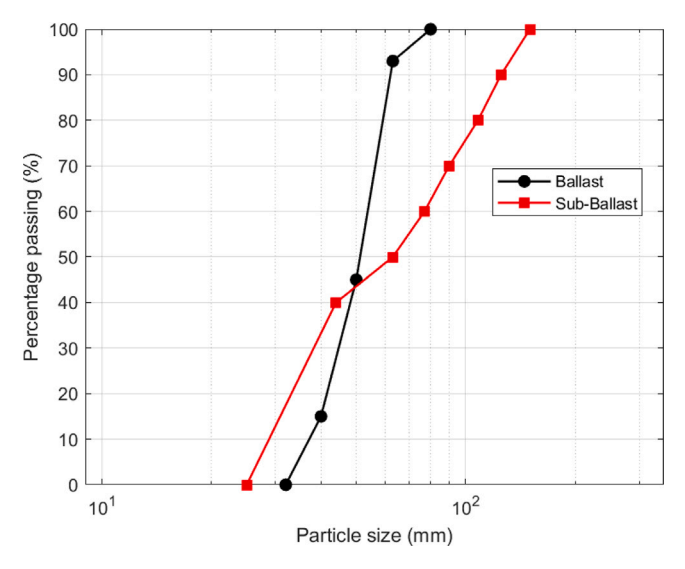


Fig. 4. Particle size distribution of the granular materials used in the DEM model.

contact between particles, in this work modelled using a linear contact law, has been shown to be reasonable for representing ballast under dynamic loading conditions (Fu et al., 2022, 2021).

2.1.2. Particle shape

The importance of realistic particle shape has been revealed in previous research (Ali et al., 2024; Nie et al., 2020; De Bono and McDowell, 2020; Xiao et al., 2023; Lu and McDowell, 2007). Therefore, clumped particles are selected to represent the ballast layer, while spherical particles are considered sufficient for the sub-ballast layer. The angular geometries of randomly selected ballast particles were obtained through a 3D scanning technique using an Artec Space Spider scanner (Ahmadi et al., 2023; Ahmadi, 2023). The scanned models were imported into PFC, where the complete 3D geometry served as input for generating clumped particle shapes. Each ballast particle was

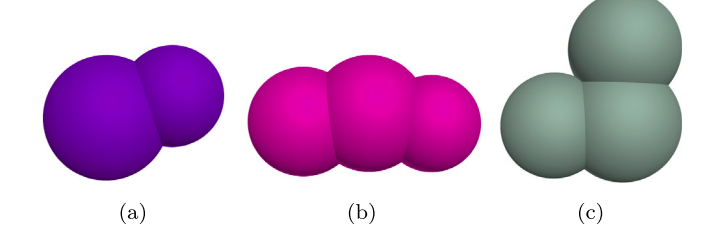
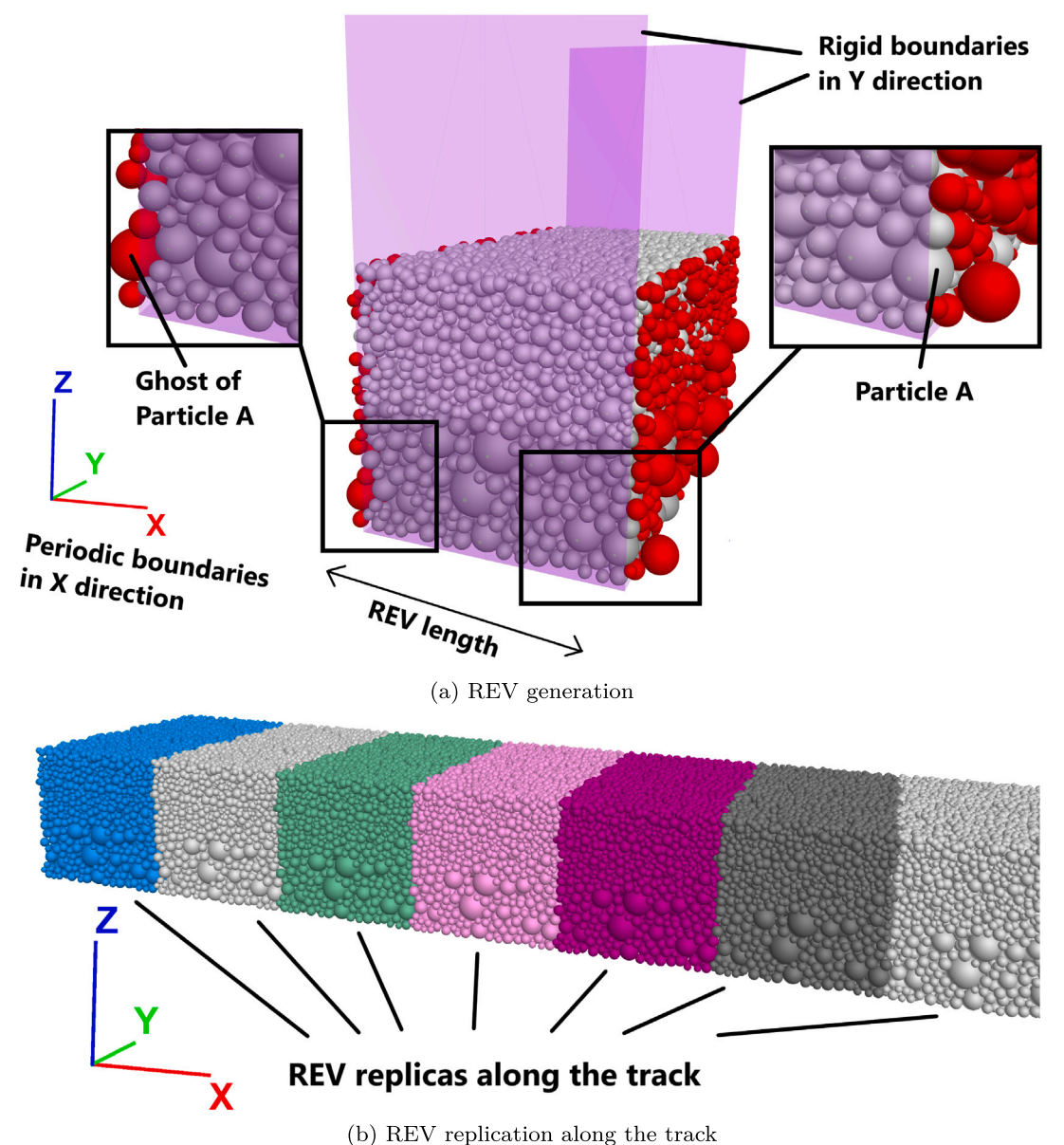


Fig. 5. Examples of clump templates used in the model.

represented by a clump template constructed from the scanned surface geometry (STL file). The clump templates were generated using PFC's bubblepack algorithm, in which a dense packing of spheres is fitted inside the ballast surface and subsequently filtered according to two main criteria: (i) sphere size ratio, where only spheres with radius greater than 0.8 of the maximum radius were retained to discard very small spheres and reduce computational cost while maintaining overall particle shape, and (ii) angular overlap distance, set to 110°, which controls the smoothness of the surface approximation. Although larger overlap distances lead to more spheres being initially generated, the size ratio filter limits the final number retained. The resulting templates consist of 2-3 overlapping spheres (pebbles) per clump, a configuration that prioritises computational efficiency while preserving the overall size, orientation, and angularity required to capture the bulk response examined in this study. While increasing the number of spheres per clump could further improve shape fidelity, the selected clump templates provide a practical balance between accuracy and computational feasibility. Some of the generated clump templates are presented in Fig. 5.

It has been confirmed that polyhedral grain models capture angularity and contact anisotropy with high fidelity. This has been demonstrated through polygon-polygon force integration over intersection facets for arbitrary polyhedra (Smeets et al., 2015), through voronoigenerated convex polyhedra with an intersecting-volume contact law and grain crushing for ballast (Eliáš, 2014), and polygonal non-smooth contact dynamics (NSCD) formulations applied to the study of ballast



(s) 102; representation along the tracin

Fig. 6. Periodic cell replication method in DEM model.

ratcheting and settlement under cyclic loading (Saussine et al., 2006; Azéma et al., 2009). In the present study, clumps consisting of 2–3 pebbles per clump are used to balance shape realism and computational tractability within a 30 m 3D DEM–FDM–FEM framework. This framework is iterated with a vehicle–track model, which enables the simulation of hundreds of axle passages and facilitates the analysis of stiffness-gradient effects in transitions.

2.1.3. Periodic cell replication method

The most computationally intensive aspects of DEM simulations include layer generation, cycling to achieve equilibrium, and layer compaction. These aspects become particularly challenging when modelling large-scale 3D models. In the present study, an advanced approach called the Periodic Cell Replication Method (PCRM) is employed, which significantly reduces the computation time. This method was originally introduced by Ciantia et al. (2018) for developing detailed 3D triaxial samples. It involves generating a small section of the target model, referred to as a Representative Elementary Volume (REV), which is then replicated throughout the model domain to construct the full-scale

system. Since creating the REV, and replicating it, requires considerably less computational effort than simulating the entire volume, this approach enables a more efficient simulation of large-scale models. Ahmadi et al. (2024b) and Ahmadi et al. (2024a) demonstrated that this method is highly effective for generating longer models of railway track in DEM simulations.

The modelling process begins with defining the boundary conditions for the REV. A rigid wall is set as the bottom boundary to prevent downward movement of the particles. The horizontal boundaries at both ends of the REV in the longitudinal direction incorporate periodic boundaries as shown in Fig. 6(a). When particles interact with these boundaries, corresponding "ghost" particles are generated on the opposite sides, ensuring continuous particle interactions throughout the model. Once the boundary conditions are established, particle generation for each granular layer begins. The sub-ballast layer is initially populated with particles based on the predefined size distribution shown in Fig. 4. These particles settle onto the bottom boundary due to gravity, accumulating until the desired layer thickness is achieved. The model then undergoes a cyclic loading to reach initial equilibrium. Due to the significant influence of compaction density on the behaviour

Table 2
Parameters of the 3D DEM-FDM track model.

Parameter	Value	Source
Track length	30 m	-
Softer side length	24 m	_
Stiffer side length	6 m	_
Model width	120 cm	_
Particle density	2700 kg/m^3	Chen et al. (2023)
Ballast layer thickness	30 cm	-
Sub-ballast layer thickness	30 cm	_
Ballast particle contact stiffness (Normal and tangential)	$1.3 \times 10^7 \text{ N/m}$	Chen et al. (2023)
Sub-ballast particle contact stiffness (Normal and tangential)	5×10^6 N/m	Chen et al. (2023)
Ballast particle friction coefficient	0.7	Chen et al. (2023)
Sub-ballast particle friction coefficient	0.5	Chen et al. (2023)
Particle friction coefficient during packing and compaction	0	_
Local damping during packing and compaction	0.7	Fu et al. (2022)
Local damping during vehicle passage	0.2	Fu et al. (2022)
Critical damping ratio during packing and compaction	0	Fu et al. (2022)
Critical damping ratio during vehicle passage	0.3	Fu et al. (2022)
Subgrade layer thickness	100 cm	_
Subgrade Young's modulus	$472 \times 10^{6} \text{ Pa}$	Nasrollahi et al. (2024a)
Subgrade density	2100 kg/m^3	Nasrollahi et al. (2024a)
Subgrade Poisson's ratio	0.25	Nasrollahi et al. (2024a)

of granular materials, a multi-layer compacting approach (Tan et al., 2024) is implemented in this study. The packing procedure begins with three sequential mini-layer generations, each compacted using pressures exceeding 200 kPa. A rigid wall is placed on top of the layers and gradually lowered, rearranging the particles and filling the voids (Ngamkhanong et al., 2021). Once the compaction is complete, the wall is lifted and removed, leaving a densely packed sub-ballast layer. This process is repeated for the three mini-layers within the sub-ballast layer. During this process, the inter-particle coefficient of friction is temporarily set to zero to facilitate particle rearrangement and compaction.

Generally, in PFC simulations of ballast packing, two primary damping methods are commonly utilised: (1) local damping, which applies a force to individual particles based on their unbalanced force and is regulated by a damping constant α , and (2) viscous (or contact) damping, which introduces a dashpot alongside the contact model that is defined by a critical damping ratio β . These damping techniques play a crucial role in managing particle dynamics and achieving steadystate conditions in dynamic analyses. Although the definitions of α and β have a strong impact on particle behaviour, determining suitable values for these model parameters is experimentally challenging for granular systems (Liu et al., 2017b; Zhang et al., 2019; Guo et al., 2020). It should be noted that the damping ratios used in this study were not calibrated ad hoc, but deliberately taken from Fu et al. (2020), who matched DEM simulations with experimental data. Their work shows that the values fall within an acceptable range, though not universally identical across different tests. Since no dedicated laboratory calibration was available in the present study, selecting values within this experimentally validated range provides the most reliable basis for our simulations. Table 2 shows the chosen parameters and their corresponding source.

Following the preparation of the sub-ballast layer, the ballast layer is added, and the same compaction procedure is applied for a 0.6 m section of the track corresponding to one sleeper bay. After compacting the REV and ensuring equilibrium, the REV is horizontally replicated along the track to construct the full model, as shown in Fig. 6(b). The number of replications depends on the width of the REV and the required length of the track model, which in this study is 24 m on the softer (ballasted) side and 6 m on the stiffer side.

At this stage, the generation of granular particles for the entire ballast and sub-ballast layers is completed and the periodic boundaries at both ends of the ballasted track are replaced with rigid wall boundaries. To characterise the initial packing, the coordination number is evaluated. For ballast, which is modelled with clumps (each clump composed of 2–3 overlapping pebbles; Fig. 5), the coordination number

is computed at the clump level (not pebbles). It is defined as the number of distinct neighbouring clumps that share at least one contact with the clump; multiple contact points between the same pair of clumps are counted only once. For the sub-ballast, represented by spherical particles, the coordination number is defined as the number of distinct contacting spheres. Based on these definitions, the average coordination numbers are 5.74 for ballast and 5.26 for sub-ballast, values that are consistent with those reported for well-compacted ballast by Suhr and Six (2020). Finally, the inter-particle coefficient of friction, and the local and critical damping ratios, are restored to their target values as specified in Table 2.

It should be emphasised that crib and shoulder ballast, critical components contributing to track stability and effective drainage, are not considered in the current study to enhance computational efficiency. Instead, the stabilising influence of the crib ballast is implicitly represented by constraining the horizontal degrees of freedom of the sleepers, thereby preserving result accuracy without necessitating explicit particle modelling. Furthermore, the shoulder ballast, which primarily functions to distribute lateral forces in curved track sections, is omitted, given that this investigation exclusively addresses straight track configurations.

2.2. Boundary conditions

The lateral boundary conditions are a key aspect of simulations of ballasted track. In the present study, the ballast and sub-ballast layers were generated using the periodic cell replication method and then bounded laterally by rigid walls. This choice was made to maintain computational feasibility for a 30 m model length including 50 sleepers.

The adoption of rigid lateral walls is consistent with previous DEM studies of large-scale railway domains. For example, Chen et al. (2023), Luo et al. (2023), and Bian et al. (2020) employed similar conditions when investigating long-term settlement under repeated loading, focusing on vertical and longitudinal responses rather than shoulder spreading. Moreover, several 2D DEM analyses (e.g., Shi et al., 2024; Fang et al., 2023; Shi et al., 2021) have used simplified lateral boundaries and nevertheless obtained acceptable agreement with experimental or field observations. These precedents reinforce that rigid-wall confinement is a pragmatic and widely adopted compromise for large-domain simulations.

Furthermore, it should be noted that railway tracks are not always free laterally in reality. For example, ballast layers on bridges, within excavated cuts, or near stations are often laterally constrained by surrounding structures. Thus, while rigid walls impose confinement,

such conditions do exist in practice and therefore cannot be considered unrealistic in all cases.

In addition, to verify that the chosen boundary conditions did not artificially stiffen the system, the static support stiffness and ballast settlement response were monitored. The static stiffness obtained from the simulations matched the range used in the Swedish railway industry (see Section 2.5). In addition, settlement magnitudes in the validated model were consistent with the experimental values reported by Bian et al. (2020) (see Section 3.2). These agreements suggest that the confinement effect was not critical for the macroscopic behaviours of interest.

To summarise, free lateral boundaries would better capture ballast shoulder deformation. However, including full shoulders in a 30 m DEM domain would have required a much larger lateral extent and fundamentally different compaction procedures for the periodic cell assemblies. This would have multiplied the computational cost to an infeasible level. The adopted rigid walls should therefore be regarded as a pragmatic compromise, in alignment with prior DEM practice, consistent with stiffness and settlement validations, and sufficient for capturing the longitudinal transition zone behaviour that is the focus of this study.

2.3. Finite difference model of subgrade

The FDM was applied through the use of the FLAC3D (Fast Lagrangian Analysis of Continua) software. In this approach, the subgrade layer is generated as a continuum layer with the material properties specified in Table 2 and then cyclically loaded to achieve initial equilibrium. Upon reaching equilibrium, the pre-assembled granular layer, constructed from replicated REVs, is placed onto the stabilised subgrade. For the combined model, a further cyclic loading is applied to attain overall system stability and equilibrium.

2.4. Railway structural components

Once equilibrium is established across all ballast and subgrade layers, rectangular rigid sleeper elements, generated in DEM, are positioned on top of the ballast layer. Rail pads, generated by spheres in DEM, are subsequently added on top of the sleepers, followed by an additional cyclic loading to achieve equilibrium. No tensile interactions are permitted at the sleeper–ballast interfaces in the DEM framework, reflecting the non-cohesive, contact-driven nature of granular media. Thus, only compressive contact forces are transmitted at these interfaces.

To accurately capture the bending behaviour of the rail structure, connected rail elements are modelled using the FDM and positioned on top of the rail pads. This modelling approach allows the rail to act as a continuous beam, effectively distributing loads across multiple sleepers, which reflects the real behaviour of railway track systems.

In many previous studies, such as (Chen et al., 2025, 2023; Bian et al., 2020), the rail structure has often been neglected by applying cyclic loading directly on the sleepers. Although this simplification reduces the complexity of the model, it overlooks an essential structural component that governs load transfer mechanisms and dynamic response. The presence of the rail significantly influences how loads are distributed, reduces local stress concentrations, and affects the overall deformation of the railway track structure.

It is particularly important to highlight that without incorporating the actual rail component, hanging sleepers cannot be realistically represented. Neglecting the rail would imply that the sleepers act as independent supports under direct loading, which contradicts in situ conditions where the rail provides a distribution of load between adjacent sleepers. Therefore, including the rail element is essential for achieving a more realistic and mechanically consistent simulation of the track behaviour.

On the stiffer side of the track model, the sleepers are fully constrained in the vertical direction to emulate the rigid boundary conditions characteristic of a tunnel or a bridge, while the rail pads are connecting the rail to the sleepers. The rail is modelled by 1D Euler–Bernoulli beam elements within FLAC3D, utilising the corresponding material properties listed in Table 2. Each sleeper bay contains four beam elements for the rail. The model is again subjected to cyclic loading until equilibrium is re-established. After achieving a stable configuration, the model parameters are adjusted to the train loading conditions as detailed in Table 2.

2.5. Multi-body system model of vehicle and finite element model of track

The parallel 2D model comprises a reduced-order nonlinear FE model of the track, accounting for gravity load, state-dependent foundation stiffness, and voided sleepers, and a discrete mass-spring-damper system of the vehicle to simulate the vertical dynamic interaction between a vehicle and the transition zone in the time domain, see Fig. 7. Tensile loads between sleepers and foundation are not considered allowing for potential loss of contact between sleeper and ballast during the vehicle passage. Based on the symmetry assumption, the model includes only the wheels running on one rail, half of the carbody, half of the bogies, one rail, half of the slab, and half of the sleepers. The 2D track model and the simulation methodology have previously been verified as reported in Nasrollahi et al. (2023). Additionally, based on the field measurements described in Nasrollahi et al. (2024a), the calibration of another similar transition zone model was carried out in Nasrollahi et al. (2024b). In the present study, the vehicle moves from the softer track section to the stiffer section, but the opposite direction of motion could also be considered.

For the vehicle, a MBS model of a freight car featuring 14 DOFs is used (Nasrollahi, 2025). However, vehicle speed was raised to 200 km/h to reduce simulation time. Two of the DOFs represent the car body motion (vertical displacement and pitch rotation). Four DOFs describe the corresponding displacements and rotations of the bogies (two DOFs per bogie), another four DOFs represent the vertical displacement of the four wheelsets, while the remaining four massless DOFs (one per wheelset) correspond to the interface with the rail (Nasrollahi, 2025). To reduce the initial pitching motion of the car body and bogies, generally induced due to the time lag between the entries of the different wheels on a track model with finite length and rigid boundaries, all wheels were placed simultaneously on the track model and the static displacement field of vehicle and track was used as initial conditions in the time integration.

The non-linear track model, shown in Fig. 7, is an FE model with rigid boundaries at both rail ends and at the lower connection points of each spring/damper model representing the ballast and subgrade. The length of the track model is 66 m, comprising 42 m of ballasted track and 24 m of the stiffer track section. The FEM model is longer than the DEM-FDM model to attenuate the influence of the boundary conditions of the track model on the dynamic vehicle-track interaction in the transition zone, ensuring an accurate representation of the wheelrail contact forces that are exported to the DEM-FDM model. For this application, it has been confirmed that the length of the track model and the number of rail nodes per sleeper bay are sufficient. As for the FDM model, the superstructure of the ballasted track comprises 60 kg/m rails, rubber rail pads, and concrete sleepers designed for axle loads up to 35 tonnes. The rail is modelled using Euler-Bernoulli beam theory with four beam elements per sleeper bay. Each rail pad is represented by a linear spring-damper element. Each sleeper in the ballasted track section is modelled as a discrete (rigid) element with only a vertical degree of freedom. In this study, the sleeper spacing L = 0.6 m is uniform, but this is not a constraint of the model. The sleepers and rail seats in the ballasted track are numbered with index i $(i = -1, -2, \dots, -(N_{\text{bays}} - 1); i < 0)$, starting from the transition, cf. Fig. 7.

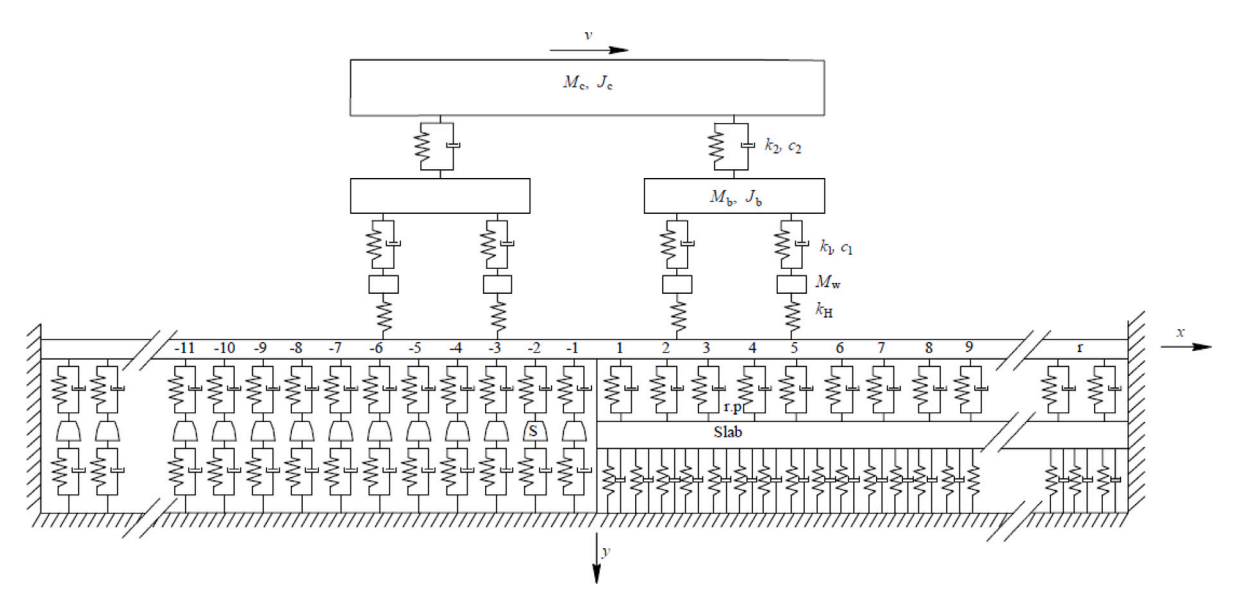


Fig. 7. Sketch of the complete vehicle and transition zone model (2D MBS-FEM model) including the softer (left) and stiffer (right) track sections. The track model on the stiffer side consists of rail (r) and a concrete slab modelled by beam elements supported by a Winkler foundation that is significantly stiffer than the support on the ballasted side. The sleepers (s) are rigid masses supported by spring-damper connections (representing ballast/subgrade) and potentially random stiffness properties. The stiffness input data for these supports are extracted from the DEM model.

Table 3
Parameters of the 2D track and vehicle models.

Track model		Vehicle model	
Parameter	Value	Parameter	Value
Track length	66 m	Vehicle speed	200 km/h
Softer side length	42 m	Vehicle axle load	20 tonnes
Stiffer side length	24 m	Car body mass, M_c	$111 \times 10^{3} \text{ kg}$
Rail density	7800 kg/m ³	Bogie mass, $M_{\rm b}$	800 kg
Rail bending stiffness	6.4 MNm^2	Wheelset mass, $M_{\rm w}$	1341 kg
Rail pad stiffness	$40 \times 10^6 \text{ N/m}$	Car body pitch inertia, J_c	$1.7 \times 10^6 \text{ kgm}^2$
Rail pad damping	5000 N⋅s/m	Bogie pitch inertia, $J_{\rm b}$	730 kgm ²
Half sleeper mass	150 kg	Wheelset inertia, $J_{\rm H}$	100 kgm ²
Sleeper spacing	0.6 m	Primary stiffness, k_1	30 MN/m
Support stiffness	Varying	Secondary stiffness, k_2	3.75 MN/m
Support damping	Varying	Primary damping, c_1	70 kNs/m
		Secondary damping, c2	10 kNs/m
		Bogie centre spacing, $\Delta_{\rm b}$	6.77 m
		Wheelset spacing, $\Delta_{\rm w}$	1.78 m

The rail seats on the stiffer track form are numbered with index i ($i = +1, +2, +3, \ldots$), cf. Fig. 7. The slab is modelled as a continuous Euler–Bernoulli beam supported by a stiff foundation. The vertical connection between each pair of adjacent nodes in different layers is modelled as a spring and viscous damper in parallel. Further input data for the ballasted track model can be found in Nasrollahi et al. (2023, 2024a,b), Ramos et al. (2024), and for the stiffer side in Aggestam and Nielsen (2019). Input data for the track model is listed in Table 3.

Most track input data, such as the properties of the rail, rail pad, sleepers, and slab, were collected from previous studies or derived from their geometrical properties, or manuals. However, the linear stiffness and damping of each sleeper support were determined by the assembled DEM-FDM model. For each sleeper position, a static load was applied on the surface of the ballast layer in the DEM-FDM model of the substructure and the corresponding displacement was calculated. In the FEM model, the ratio between the applied load and the calculated displacement is used as the support stiffness at that particular sleeper. The ratios between stiffness and viscous damping is similar to the value suggested by Nielsen (Nielsen, 2008).

Based on the assembled stiffness matrix for the track model, the static stiffness at rail level along the track was calculated, see Fig. 8. As expected, the stiffness at rail level displays a periodic pattern due to the discrete positions of the rail supports on both sides of the transition.

Further, a significant stiffness gradient associated with the change in track form is observed.

The vehicle has an axle load of 20 tonnes, corresponding to a static wheel load of 98 kN. The stiffness between each wheel and its corresponding massless DOF is modelled using a nonlinear Hertzian contact stiffness. The parameter values used in the vehicle model are provided in Table 3. This vehicle model has been verified against a more extensive 3D model developed using the commercial software GENSYS (Nasrollahi et al., 2023).

For the initial state of the transition zone, including the stiffness gradient and variations in support stiffness according to Fig. 8, but assuming there are no irregularities or misalignment in longitudinal level across the transition, part of the simulated time history of the vertical wheel–rail contact force for the leading wheel of the leading bogie is illustrated in Fig. 9. The direction of the vehicle is from the softer track (negative rail seat numbers) to the stiffer track (positive rail seat numbers). Each passing of a sleeper leads to a small increase in contact force since the track stiffness is higher above the sleepers. It can be concluded that the stiffness gradient at the transition contributes to a transient in the dynamic load for each passing wheel. The transition also induces a pitching motion of the vehicle leading to the superposition of a low-frequency variation in contact force. In the next step of the simulation methodology, the set of calculated time histories

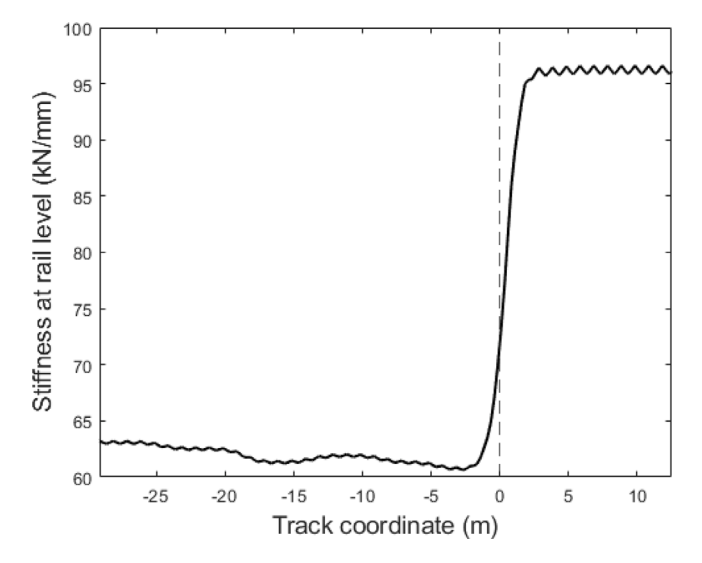


Fig. 8. Static track stiffness at rail level along the transition calculated using the FEM model. The vertical line indicates the position of the transition. Rail seat numbers are positive on the stiffer track form.

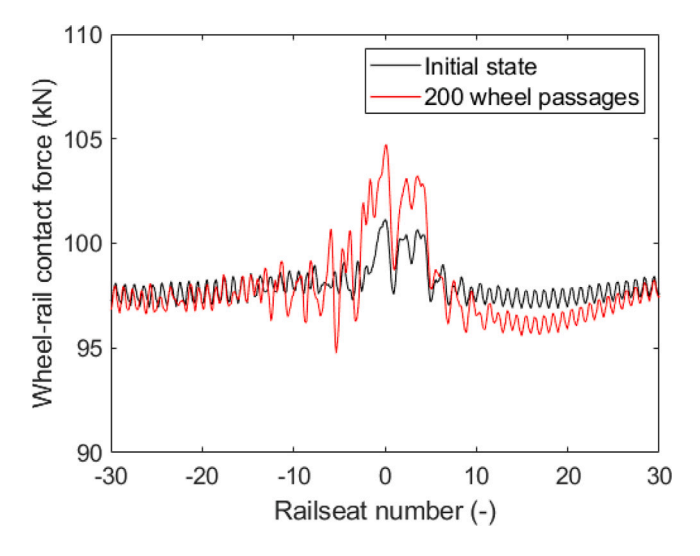


Fig. 9. Time history of vertical wheel–rail contact force for the leading wheel of the leading bogic calculated using the 2D MBS-FEM model. The transition between the softer and stiffer track sections is located at rail seat 0.

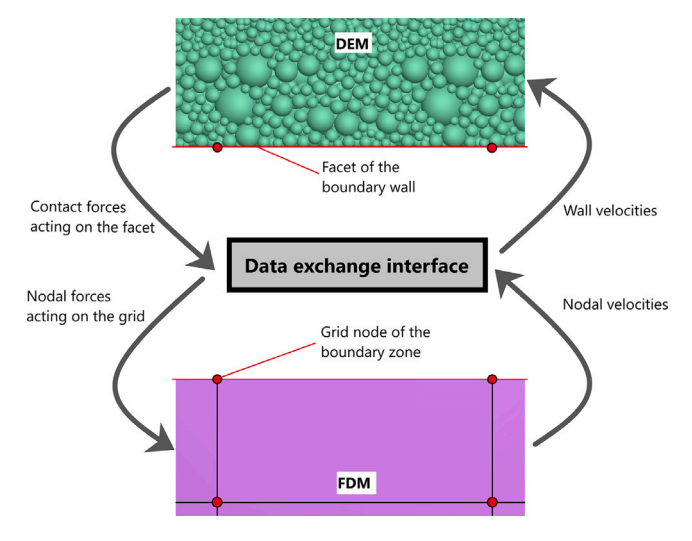


Fig. 10. DEM-FDM domain integration.

of wheel–rail contact forces for the complete vehicle model is used as input to the FEM–FDM model to predict the resulting track settlement, see Section $2.6\,$

2.6. Integration of hybrid DEM-FDM-FEM model

Once all components of the hybrid model have been generated, the DEM model implemented in PFC3D and the FDM model in FLAC3D are integrated, enabling a hybrid simulation that combines discrete granular behaviour with continuum models. At each time step of the simulation, the model is partitioned into two domains: the DEM domain, representing the granular layers together with the sleepers and rail pads, and the FDM domain, representing the subgrade layer and the rail. Data transfer between the domains is facilitated through a specialised interface layer, where DEM particles interact with the FDM mesh. Here, boundary conditions and contact laws are implemented to ensure seamless interaction. Contact forces from the DEM, derived from simulated particle interactions, are transmitted to the FDM domain. which in turn computes deformations and returns the corresponding displacement and velocity data. These are then used to update the motion of the DEM particles, as illustrated in Fig. 10. This method of coupling the two domains has been utilised extensively in previous research, demonstrating the suitability of the approach (Shi et al., 2024; Tizpa et al., 2023; Shao et al., 2022; Cui et al., 2021; Shi and Chen, 2021; Jia et al., 2018). Table 2 presents the material properties employed in the hybrid model.

All the methods and models described above are integrated according to the flowchart in Fig. 3 to form the complete DEM-FDM-FEM model depicted in Fig. 2. In an iterative procedure, wheel-rail contact forces from the FEM model are used as input in the DEM-FDM model to predict the accumulated differential settlement along the transition zone. In the next iteration step, this settlement is used as input in the FEM model to calculate a new set of wheel-rail contact forces, which are then used as input in the DEM-FDM model, etc.

3. Validation of the model

Before a detailed demonstration of the integrated DEM-FDM-FEM model is presented in the next section, key findings from previous validation exercises are briefly summarised here. In addition, parts of the DEM-FDM model that have not been validated in earlier works are verified against the FEM model.

Based on field measurement data, the FEM track model was calibrated in Nasrollahi et al. (2024a,b, 2023), Nielsen (2008), while the vehicle model was verified by comparing it with a more advanced version in the MBS software GENSYS, see Nasrollahi et al. (2023).

3.1. Substructure-DEM model

In order to validate the substructure part of the model, the full-scale physical test of a ballasted track for high-speed railway traffic, as presented by Bian et al. (2020), was chosen for its robustness and accuracy. The calibration methodology and input parameters were obtained from Chen et al. (2023), ensuring precision and reliability. The combined use of the physical test by Bian et al. (2020) and the parameters presented by Chen et al. (2023) enables a comprehensive analysis of the behaviour of ballasted track.

The test set-up developed by Bian et al. (2020) included a subballast layer, a ballast layer, eight concrete sleepers with rail pads and spacing 0.6 m, over a width of 2.6 m. The 0.4 m thick ballast layer contained particles with the fraction 16 mm to 64 mm, while the 0.7 mm thick sub-ballast layer included particles sized 0.1 mm to 45 mm. Further details are available in Bian et al. (2020). In the test, three sensors were used to measure stress and vibration velocities. A soil pressure sensor (S1) was installed 30 cm below the sleeper within the ballast layer. Two vibration velocity sensors were placed on the sleeper

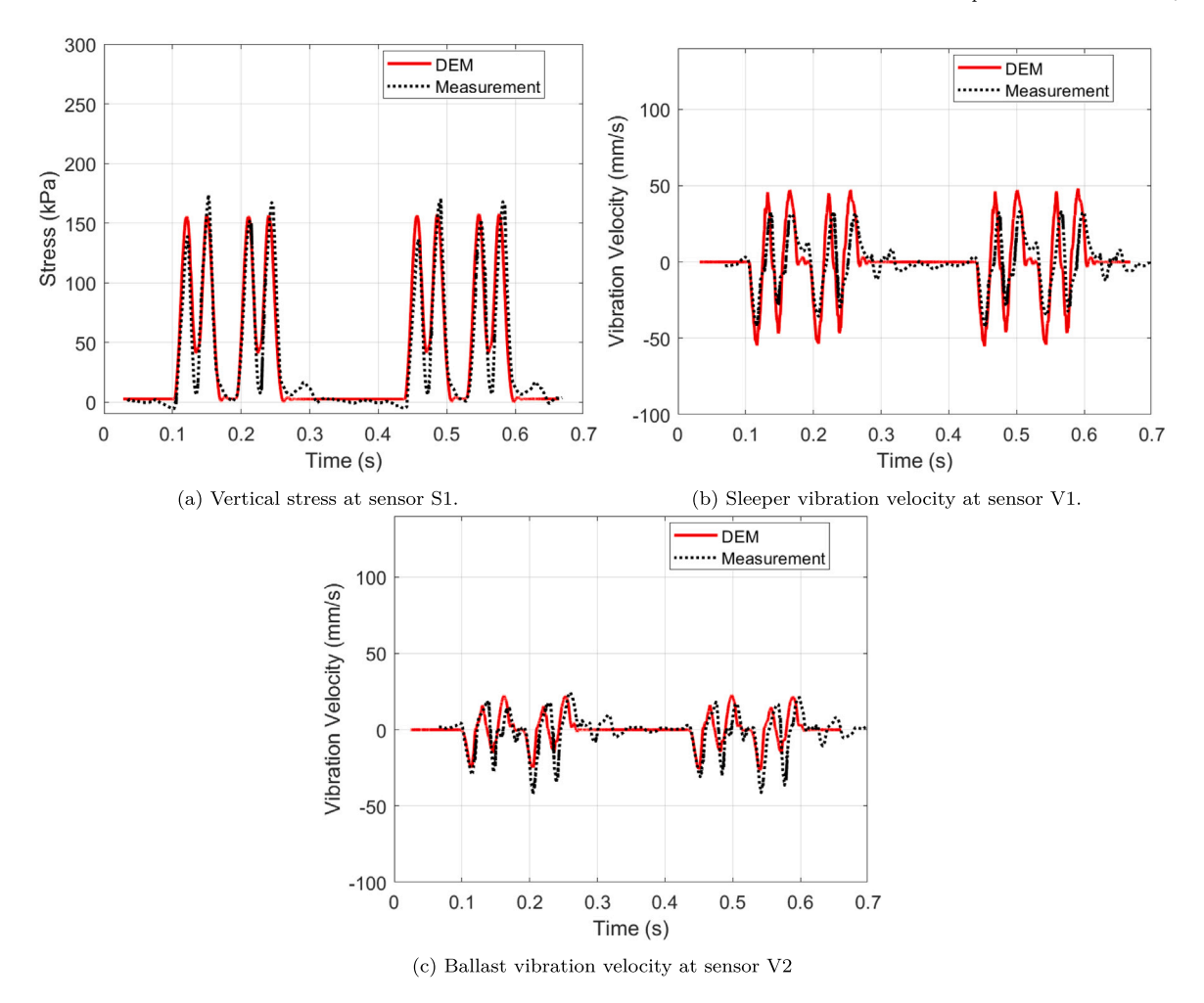


Fig. 11. Validation of DEM model of railway substructure against physical measurements. From Ahmadi et al. (2024b).

in the middle of the set-up and on top of the ballast layer between two sleepers, respectively. A set of eight hydraulic actuators was employed to impose a time-variant loading of the set-up, simulating a vehicle travelling on the track. Each actuator applied the load of the train that each sleeper carried.

A DEM model was developed to replicate the described physical model test. The superstructure was constructed following the procedure outlined in Section 2. Further details on the superstructure model can be found in Ahmadi et al. (2024b). A comparison of the results between the DEM model and the physical test is shown in Fig. 11. Stresses in the ballast were computed following the method of Christoffersen et al. (1981), by embedding predefined measurement spheres at the same depth and lateral positions as the sensors in Bian et al. (2020), where contact forces and branch vectors were accumulated and the average stress obtained as

$$\sigma = -\frac{1}{V} \sum_{c=1}^{N_c} \mathbf{F}^c \otimes \mathbf{L}^c, \tag{1}$$

with V denoting the averaging volume, N_c the number of contacts, \mathbf{F}^c the contact force, and \mathbf{L}^c the branch vector. In parallel, vibration velocities were determined by averaging the instantaneous velocities of all particles within a defined *measurement volume* (e.g., $0.2\times0.2\times0.3$ m³) located in the ballast layer, consistent with the procedure of Bian et al. (2020). Note that the motion of individual ballast particles is influenced by the inter-particle contact states. Due to differences in contact states between laboratory tests and DEM modelling, it is challenging to achieve perfect agreement in particle movements. A recent study by Liu et al. (2017a) has shown that while the motion

intensities between DEM simulations and SmartRock sensor measurements can differ significantly, the overall vibration signatures remain stable and comparable. This confirms that DEM models can capture the key kinematic behaviour even if quantitative differences exist in displacement and velocity magnitudes.

3.2. Superstructure-DEM-FDM model

To validate the structural integrity and accuracy of the DEM-FDM coupling in simulating railway track behaviour, a simplified model of railway superstructure was constructed. This model excludes the ballast and subgrade layers to focus solely on the rail, rail pads, and sleepers. The sleepers and railpads are modelled in DEM, while the rail beam is modelled in FDM. The model response is benchmarked against the FEM model, assuming a rigid foundation.

In the DEM-FDM model, the vertical displacement of 20 sleepers (12 m) was constrained, with rail pads and a section of rail mounted on top of them. To evaluate the static performance of the structural elements, a vertical static load of 100 kN was applied above the sleeper at the centre of the model, as illustrated in Fig. 12(a). The resulting responses in terms of the distribution of load between the rail pads, bending moment along the rail, and vertical deflection of the rail, were evaluated using both the DEM-FDM and FEM models.

Fig. 12 presents a comparison between the simplified DEM-FDM and FEM models. The results are in good agreement between both models in terms of both magnitude and overall trend. Also in terms of load distribution between rail seats (Fig. 12(b)), the percentage distribution of vertical load shows good agreement. As expected, the central three

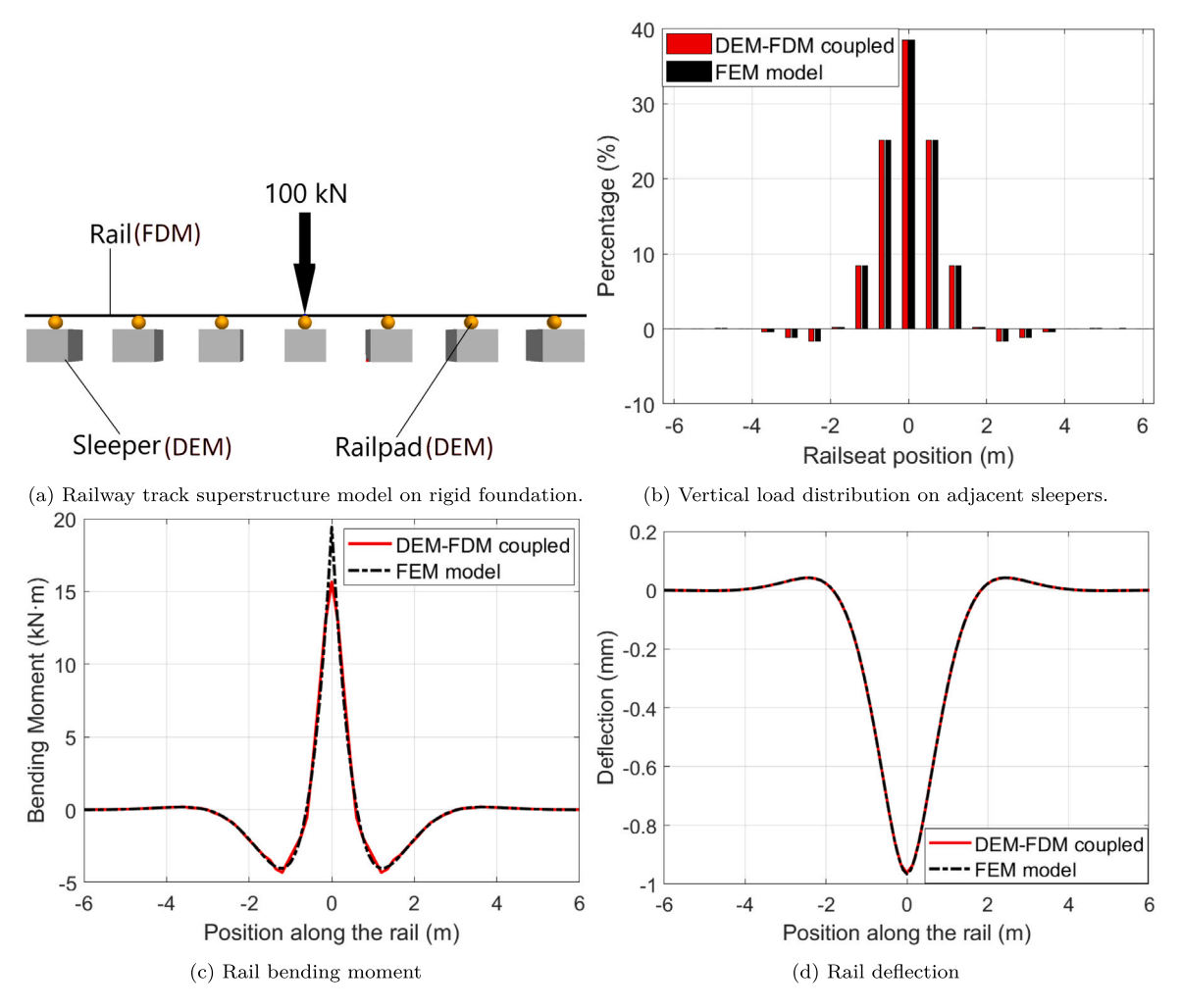


Fig. 12. Validation of DEM-FDM superstructure model for a stationary static load.

rail pads carry the highest proportion of the load with the force distribution tapering off symmetrically. Regarding the rail bending moment (Fig. 12(c)), the DEM-FDM model captures a maximum value of 16 kNm while the FEM model gives a maximum value of 19 kNm. Besides the offset in maximum value, the appearance is very similar. The symmetry and magnitude of the rail bending moment on either side of the load further confirm an accurate load transmission along the rail structure. Similarly, the vertical deflection of the rail (Fig. 12(d)) shows an identical profile between the two models.

3.3. Full DEM-FDM model

To verify the complete DEM-FDM track model, including both the superstructure and substructure, calculated short-term dynamic responses are compared with those from the calibrated FEM model. A one-way traffic scenario is considered, in which the vehicle model travels at 200 km/h, moving from the softer track to the stiffer track. Predicted time histories of rail bending moments above sleepers -5 and -20 are presented in Figs. 13(a) and 13(b). Furthermore, time histories of simulated rail seat loads due to the passage of the same vehicle are compared in Figs. 13(c) and 13(d).

Good agreement is observed between both models in terms of rail seat loads and rail bending moments. The magnitudes of the calculated sleeper displacements (not shown here) from both models were also found to be essentially similar, despite the DEM-FDM model being more comprehensive compared to the simpler FEM model, while the FEM model is longer than the DEM-FDM model. Based on the overall good

agreement in these results, the FEM-DEM-FDM model is used for further studies in this paper.

4. Demonstration of hybrid DEM-FDM-FEM model

Using the integrated discrete–continuum model described above, a numerical methodology for simulating the mechanisms of differential settlement in a railway transition zone will be demonstrated. For a vehicle model traversing the stiffness gradient from the softer ballasted track to the stiffer track form, a comprehensive analysis has been performed to investigate the dynamic response and load distribution across the different track layers due to the evolving irregularity in vertical track geometry. In the initial state of the transition zone, it is assumed that the track is perfectly level in vertical alignment (and the wheels are perfectly round). Results are presented for short-term responses after 100 and 500 axle passages, facilitating an evaluation of the influence of the progressive permanent deformation of the substructure caused by the cyclic, and in terms of magnitude and frequency content, changing vehicle load.

4.1. Short-term analysis

Calculated short-term dynamic responses from the top level (rail) down are presented in this section. The full vehicle model, as shown in Fig. 7, was considered in the simulations. However, only the track response due to the leading bogie, traversing the transition zone in the direction from the softer ballasted track to the stiffer track form

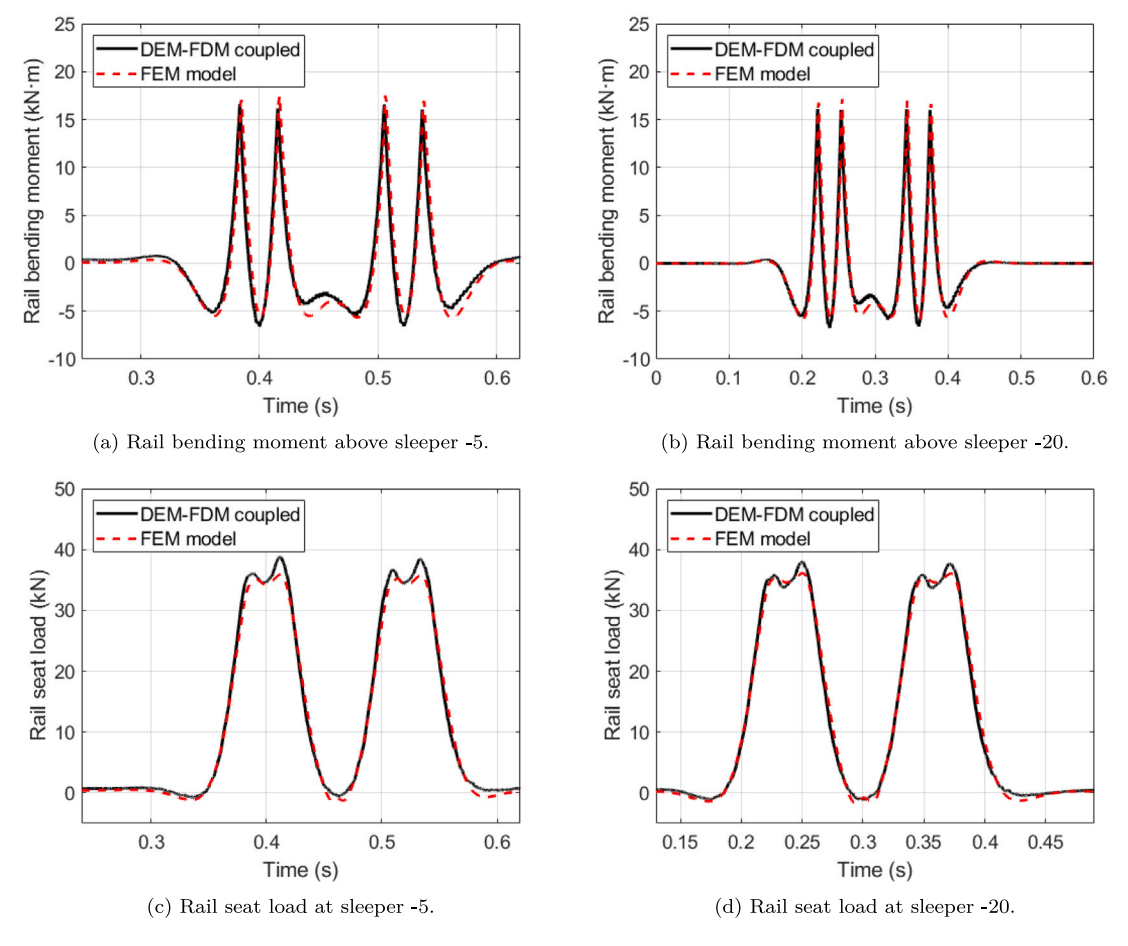


Fig. 13. Validation of integrated DEM-FDM model versus FEM model for a moving dynamic vehicle load.

at speed 200 km/h, will be discussed here. As the vehicle load is distributed from the rail down to the ballast, the responses of the rail, rail pad, sleeper, and ballast layer are examined to investigate the mechanisms of load transfer and vibration in a transition zone.

Recent studies have shown that the ballast layer exhibits the highest levels of permanent and transient deformation, confirming that it is the most vulnerable layer in the substructure, see Chen et al. (2024), Unsiwilai et al. (2024). The contact states of individual ballast particles change with cyclic loading, resulting in particle movement. This accumulation complicates efforts to assess ballast performance using particle-scale metrics, particularly under long-term operating conditions.

In order to assess the response of the ballast layer, a specific volume of particles located directly beneath each sleeper was selected for further analysis. Vertical velocity and acceleration were calculated for each particle within the specified volume. However, given the significant variations in the dynamic response of the particles within the volume due to their unique shape, mass, and orientation, reliance on individual values would introduce a high degree of variability in the results. Thus, for each time step, the arithmetic averages of the vertical velocity and acceleration evaluated over all ballast particles within the volume were calculated, providing single representative values for the ballast behaviour beneath each sleeper. This averaging process reduces the influence of local anomalies and particle-specific effects, ensuring that the resulting values are more statistically robust and independent of specific particle arrangements. This method has been shown to increase the reliability of the analysis in cases where heterogeneity occurs in granular media.

Ballast acceleration was obtained directly from the DEM output using Newton's second law, which is solved explicitly at each time step for every particle,

$$m_i \mathbf{a}_i = \sum \mathbf{F}_i \tag{2}$$

where m_i is the particle mass, \mathbf{a}_i its acceleration, and $\sum \mathbf{F}_i$ the sum of contact and body forces acting on the particle. To evaluate the macroscopic response of the ballast layer rather than the behaviour of individual particles, predefined measurement volumes (e.g., $0.2 \times 0.2 \times 1.2 \, \mathrm{m}^3$) were introduced beneath each sleeper in the ballast layer. For every time step, the vertical velocities and accelerations of all particles inside each measurement volume were extracted and their arithmetic averages computed. This averaging reduces the influence of local anomalies and particle-specific variations caused by differences in shape, mass, and orientation, resulting in statistically robust representative values for ballast acceleration. The averaged time histories obtained in this way are reported. This procedure ensures that the computed ballast response reflects the collective behaviour of the granular assembly and is consistent with practices commonly adopted in DEM studies of heterogeneous granular media.

4.1.1. Rail response

Time histories of vertical rail displacement and rail bending moment above three selected sleepers, due to the two wheel passages of the leading bogie, are presented in Fig. 14. The calculated vertical rail displacements (Fig. 14(a)) and rail bending moments (Fig. 14(b)) at rail seats -13 and -3, located on the softer (ballasted) track side, and at rail seat +7 on the stiffer track form, correspond to the two cases where the vehicle model is traversing the transition zone considering the irregularity in vertical track geometry after 100 and 500 axle passages, respectively. For clarity and consistency in comparing the displacements after 100 and 500 passages, the permanent settlements

accumulated from earlier passages have been subtracted from the response to isolate and analyse each bogie passage individually.

As illustrated in Fig. 9, the influence of the stiffness gradient at the transition on the wheel-rail contact force becomes more evident after multiple axle passages, owing to the evolving irregularity in track level. The irregularity is exacerbated by the densification of the ballast and sub-ballast during the initial load cycles (consolidation of the subgrade layers is not considered). Greater settlement occurs at sleepers in proximity to the transition compared to other locations due to significantly higher sleeper-ballast contact pressures in this area, see Section 4.1.3. Displacements of both rail and sleepers adjacent to the transition are greater than elsewhere. This is illustrated in Fig. 14(a), where the rail at rail seat -3 exhibits a larger displacement than at rail seat -13. Notably, rail seat -13, located farther away from the transition, serves as a reference for the response of the embankment under the cyclic loading. Here, only a minimal influence of the stiffness gradient and the accumulated settlement is noted, as the change in displacement between 100 and 500 axle passages is negligible. On the stiffer side, the rail at rail seat +7 shows a smaller displacement, attributable to the higher support stiffness on this side.

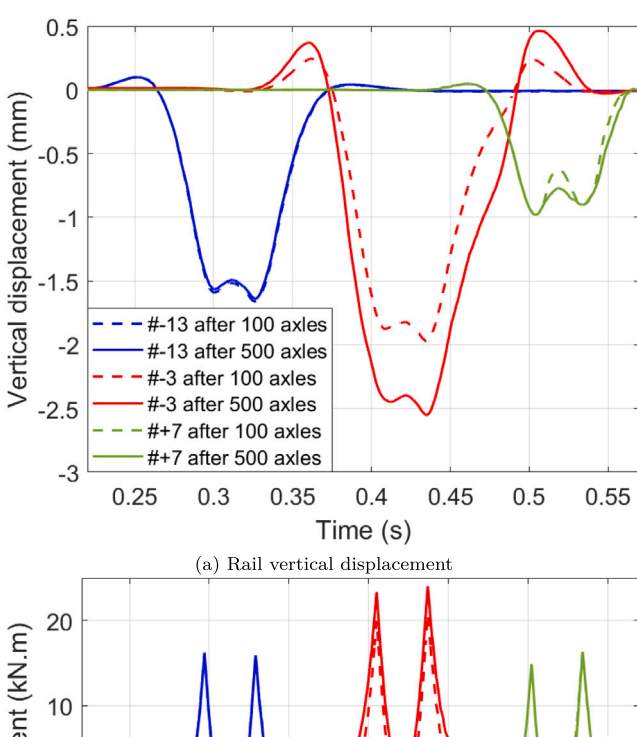
Time histories of the rail bending moment above rail seats -13, -3, and +7 are shown in Fig. 14(b). The maximum rail bending moment above rail seat -3 is higher than at rail seats -13 and +7, indicating that sleeper -3 has a softer support compared to the other two. The rail bending moment at rail seat -3, before the passage of the vehicle, is not zero, since the rail is suspended by the stiffer track form once there is some accumulated settlement on the ballasted side. The combination of higher, and over time increasing, vertical displacements and rail bending moments in the transition zone highlights the need for improved track design in this region. In the long term, the deterioration of the sleeper supports and the evolving irregularity in vertical track geometry may lead to the risk of rail fatigue and the initiation of cracks (Talebi et al., 2024), increased maintenance demands, and a reduction in the overall service life of the track.

4.1.2. Rail seat loads

The maximum values for rail seat loads after 100 and 500 axle passages, evaluated across all sleepers along the transition, are shown in Fig. 15(a). A significant variation in load is observed at the transition between the ballasted track and the stiffer track form. The first sleeper on the stiffer track form is subjected to the highest loading. Furthermore, there is a local maximum in load for sleepers -8 through -6 on the ballasted side, leading to a local maximum in differential settlement.

The lower loads in front of the transition, followed by an abrupt increase immediately after the transition, signifies that sleepers -1 to -3 are suspended by the section of the rail on the stiffer track form, thereby preventing significant displacement. This behaviour suggests the formation of gaps beneath these sleepers. As shown by Nabochenko et al. (2024), even minor gaps beneath sleepers can significantly amplify impact forces on ballast particles, ultimately resulting in increased settlement over time. As a result, the load is redistributed among adjacent sleepers. Consequently, the first sleeper on the stiffer side (sleeper +1), along with sleepers from number -4 and onwards (in the negative direction on the ballasted side), carry not only their own share of the gravity load and vehicle load but also an additional load transferred from the suspended sleepers. This phenomenon occurs in conjunction with higher dynamic loads, which are caused by the lowfrequency pitching motion of the vehicle as it traverses the stiffness gradient and the misalignment in rail level at the transition.

Fig. 15(b) shows the simulated time histories of selected rail seat loads. Negative rail seat loads correspond to forces acting upwards, away from the ballast, indicating a momentary loss of contact between the sleeper and the ballast layer. Comparing the dynamic response of the track after 100 and 500 axle passages, the load distribution changes significantly (cf. Fig. 15(a)) and becomes more pronounced as the number of axle passages increases.



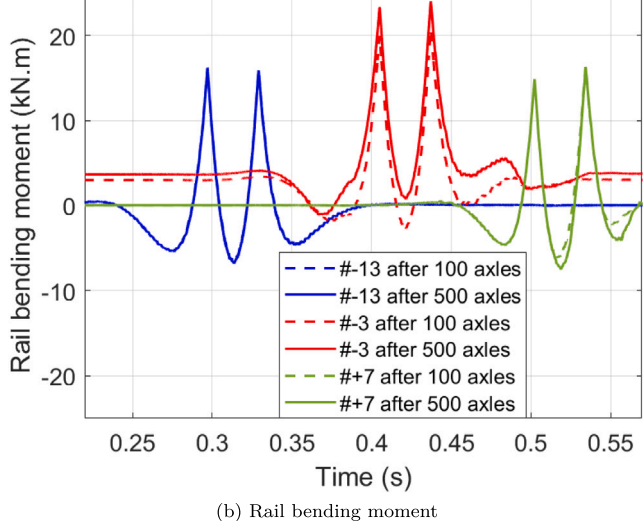
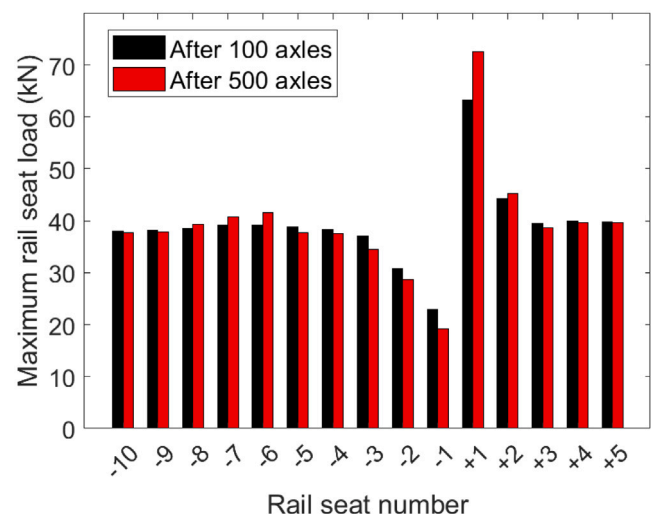


Fig. 14. Time histories of simulated rail responses at selected rail seats adjacent to the transition during a bogie passage, considering the differential settlement after 100 and 500 axle passages, respectively.

4.1.3. Sleeper and ballast responses

The predicted accumulated settlement per sleeper along the ballasted track after 100 and 500 axle passages, and the corresponding maxima in sleeper–ballast contact force in the unloaded condition due to gravity load only, are plotted in Figs. 16(a) and 16(b). It is evident that sleepers –1 through –5 carry smaller partitions of the gravity load of the superstructure. This load is transferred to sleepers –6 through –9 on the ballasted side, and to sleeper +1 on the slab side (not shown here). Due to the more settlement on the ballasted side after several axle passages, sleepers –1 through –5 eventually become fully suspended by the rail, thereby increasing the load carried by their adjacent sleepers.

For sleepers -13 and -3, the time histories of the sleeper-ballast contact force from the FEM model, as well as the sleeper velocity, sleeper acceleration, ballast velocity, and ballast acceleration from the DEM-FDM model, are presented in Figs. 16(c), 16(d), 17, and 18, respectively. In the unloaded state after 100 axle passages, sleeper -3 carries a preload of approximately 0.5 kN due to the weight of the superstructure, see Fig. 16(b). This preload persists until the leading wheel reaches a position a few sleepers ahead of this sleeper (see Fig. 16(c)). At this point, the sleeper-ballast contact is lost due to upward



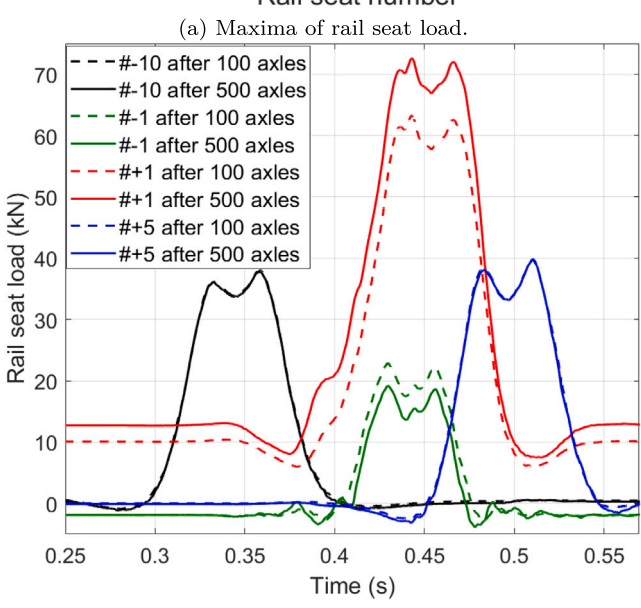


Fig. 15. Simulation of rail seat loads after 100 and 500 axle passages. Negative sleeper numbers correspond to the softer track section, while positive sleeper numbers correspond to the stiffer track form.

(b) Time histories of rail seat load.

bending of the rail (corresponding to a zero sleeper-ballast contact force), as indicated by the shaded region. Contact is re-established when the leading wheel reaches a position closer to sleeper -3, generating a new contact force with an impact. There are further intervals of lost contact at times between the two bogies in the full vehicle model and after the trailing bogie has passed.

Fig. 17 shows the corresponding time histories of vertical velocity and acceleration for sleepers -13 and -3. Sleeper -3, located closer to the transition, shows substantially higher vibration levels compared to sleeper -13. This difference becomes even more pronounced with increasing number of axle passages. Soon before the leading wheel of the leading bogie reaches sleeper -3, while there is no contact between sleeper and ballast as indicated by the left shaded area (cf. Fig. 16(c)), both sleeper velocity and acceleration are positive corresponding to an upward motion due to the lifting of the rail. This continues until the sleeper regains contact with the ballast, whereby both velocity and acceleration become negative, indicating downward motion. A similar upward sleeper motion occurs when the trailing wheel of the leading bogie has passed the sleeper as indicated by the right shaded area.

Similarly, in Fig. 18, the average time histories of velocity and acceleration for the defined measurement volumes within the ballast assembly beneath sleepers -13 and -3 indicate that levels of substructure vibration increase with decreasing distance to the transition, particularly after 500 axle passages. The pronounced spikes are indicative of a sudden regained contact between sleeper and ballast as the leading wheel of the leading bogie is passing over. Prior to the arrival of the leading wheel, the ballast exhibits a state of quiescence, devoid of any vibration. This signifies an absence of both sleeper-ballast contact and motion within the ballast. Subsequently, the sleeper re-establishes contact with the ballast, resulting in downward displacement into the ballast layer. Subsequent axle passages gradually create an evolving voiding on the ballasted side, thereby affording the ballast particles below sleeper -3 greater mobility, resulting in brief surges of higher acceleration and velocity whenever an axle (or bogie) passes. While the ballast below sleeper -13 exhibits increased acceleration beyond 100 axle passages, its magnitude remains significantly lower, indicating less progressive settlement for an equivalent number of load cycles.

It is clear that the signatures of velocity and acceleration response do not change much for sleeper -13. This observation implies that the support conditions far from the transition remain comparatively stable, with minimal additional ballast gaps forming beneath these sleepers due to more uniform settlement along this section of the transition. This reduces the likelihood of abrupt load transfers and large inertial effects, limiting the peak levels of sleeper velocity and acceleration. In contrast, the larger amplitude accelerations and velocities for sleeper -3 accelerate ballast wear, promote the formation of voids, and increase the demands on track maintenance. As discussed by Shi et al. (2024), increased friction energy within the ballast layer correlates with accelerated particle wear. Therefore, zones with unsupported sleepers, where relative particle motion and impact are intensified, are likely to experience higher rates of ballast degradation.

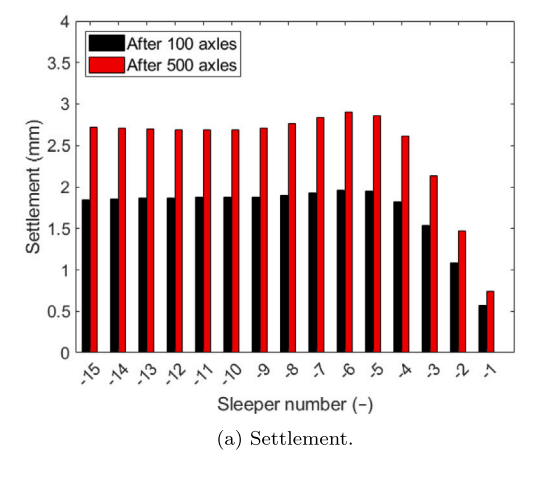
From a broader operational perspective, the persistent increase in vibration for sleeper -3 between 100 and 500 axles indicates that track segments adjacent to transitions are prone to progressive deterioration. Monitoring such sleepers over repeated load cycles becomes critical for early detection of void growth and incipient track geometry problems, see Nasrollahi et al. (2024a), Milosevic et al. (2023). In contrast, regions, such as at sleeper -13, located farther from the transition, remain substantially more stable and exhibit far smaller changes in vibration levels over time, affirming that they are less susceptible to long-term settlement-driven vibration issues.

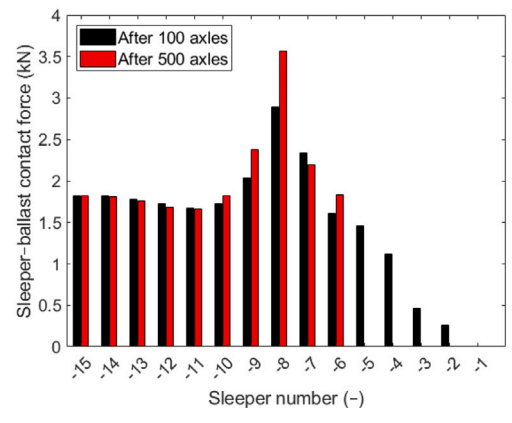
These findings confirm that differential settlement is most severe near the transition on the ballasted side. The accumulation of load cycles tend to worsen the differential settlement for some sleepers in the transition zone, increasing the void between sleeper and ballast, and transferring more dynamic load to adjacent sleepers. As a consequence, the ballast experiences increased vibration, with amplified velocity and acceleration peaks that indicate evolving void formation. In turn, the less affected sleepers far from the transition settle more slowly and uniformly, reflecting a more consistent load distribution away from the interface with the stiffer track form.

4.2. Long-term analysis

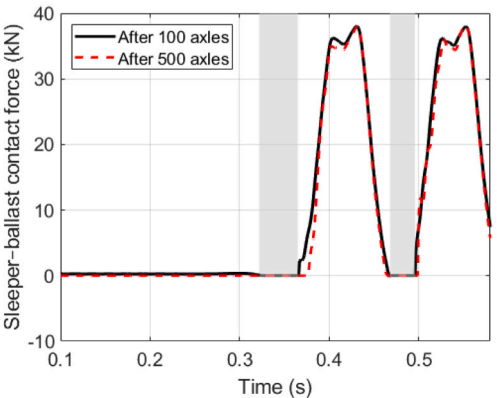
As discussed in Sections 2.5 and 4.1.3, the stiffness gradient in the transition zone causes a dynamic excitation of the vehicle–track system, leading to higher rail seat loads and more settlement (a local maximum) in the ballast below some sleepers adjacent to the transition, typically around sleepers 6 to 8 from the transition, as indicated in Fig. 15(a). This initiates a feedback loop, with increased dynamic excitation that results in higher rail seat loads and sleeper–ballast contact forces, causing further differential settlement.

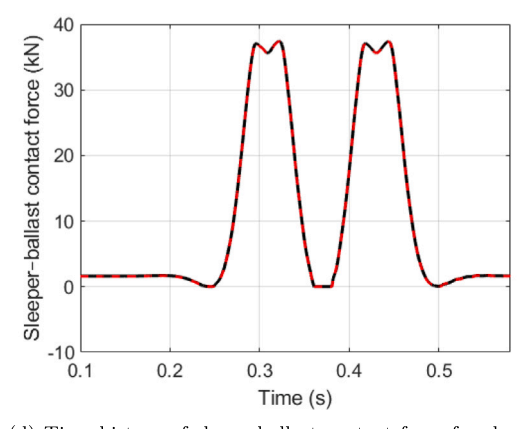
Notably, the development of voided sleepers near the transition results in a load redistribution to adjacent sleepers (towards higher sleeper numbers). Consequently, greater settlements are generated at





(b) Sleeperballast contact force due to gravity load.





- (c) Time history of sleeperballast contact force for sleeper -3. Full vehicle model.
- (d) Time history of sleeperballast contact force for sleeper -
- 13. Full vehicle model.

Fig. 16. Simulation of sleeper-ballast contact forces after 100 and 500 axle passages: (a) settlement per sleeper, (b) sleeper-ballast contact forces due to gravity load, (c) time history of sleeper-ballast contact force for sleeper -3 due to gravity load and vehicle load; (d) time history of sleeper-ballast contact force for sleeper -13 due to gravity load and vehicle load. The shaded areas indicate the intervals at which sleeper -3 has lost contact with the ballast (only illustrated for 100 axle passages).

these adjacent sleepers, gradually leading to a slight shift of the location with the maximum settlement further away from the transition. Fig. 19 presents the simulated rail displacement due to gravity load (but without vehicle load) along the track at three stages: the initial condition (before any vehicle passage), after 100 axle passages, and after 500 axle passages. In Fig. 19, the two track forms are visually distinguished by a shaded region.

In the initial state (black solid line), the rail level remains relatively uniform with a minimal variation in displacement along the track, indicating a well aligned track geometry across both the ballasted side and the stiffer track form. However, due to the difference in support stiffness on either side of the transition, there is a misalignment in longitudinal level of about 0.4 mm at the transition. After 100 axle passages (red dashed line), a higher but still relatively uniform permanent displacement of the rail is observed on the ballasted side. In addition, a local maximum in settlement is starting to appear for the sleepers at about 2.9 m from the transition. The effect of the accumulated loading becomes significantly more apparent after 500 axle passages (red solid line). Here, the level of uniform permanent rail displacement far from the transition has increased even further due to substantial settlement within the softer track section. The local maximum in permanent displacement at approximately 3 m from the transition has gradually been magnified with a maximum settlement now reaching nearly 3 mm.

Mitigation measures such as auxiliary rails, a reinforced embankment substructure, or a transition wedge to raise track stiffness at rail level on the ballasted side, or implementing softer rail pads on the stiffer track form, could be considered in the transition zone design to better match the stiffnesses between the two track forms, thereby reducing the stiffness gradient and dynamic load amplification, and preserving track integrity over time. While this is not in the scope of this paper, the model could incorporate some of these designs.

As discussed by Chen et al. (2023), while the modelling framework presented here effectively captures the qualitative behaviour of track settlement and dynamic responses in ballasted track, the predicted magnitudes of settlement may not precisely replicate field measurements (for a given accumulated traffic load, the settlement predicted here may typically exceed that measured in the field). This is primarily due to several modelling assumptions and simplifications. The DEM, while powerful in capturing particle-scale interactions, inherently includes some limitations in its constitutive formulation. Simplifications such as idealised particle shapes and sizes, as well as restricted model boundaries, contribute to deviations from in situ behaviour. Additionally, it has been established that the dynamic loads exerted by individual sleepers on the ballast are contingent on factors such as variations in train speed, axle load, vehicle configuration, the stiffness of the ballast (which, in turn, is influenced by the sleeper-ballast contact stress), and track alignment (Indraratna and Ngo, 2018). Further, this study has not considered variations in ballast properties (e.g., due to the degradation or breakage of ballast particles). Consequently, the results presented here should be interpreted as a qualitative investigation of the mechanisms that drive long-term ballast degradation and settlement, rather than a precise quantitative prediction of in situ levels of settlement.

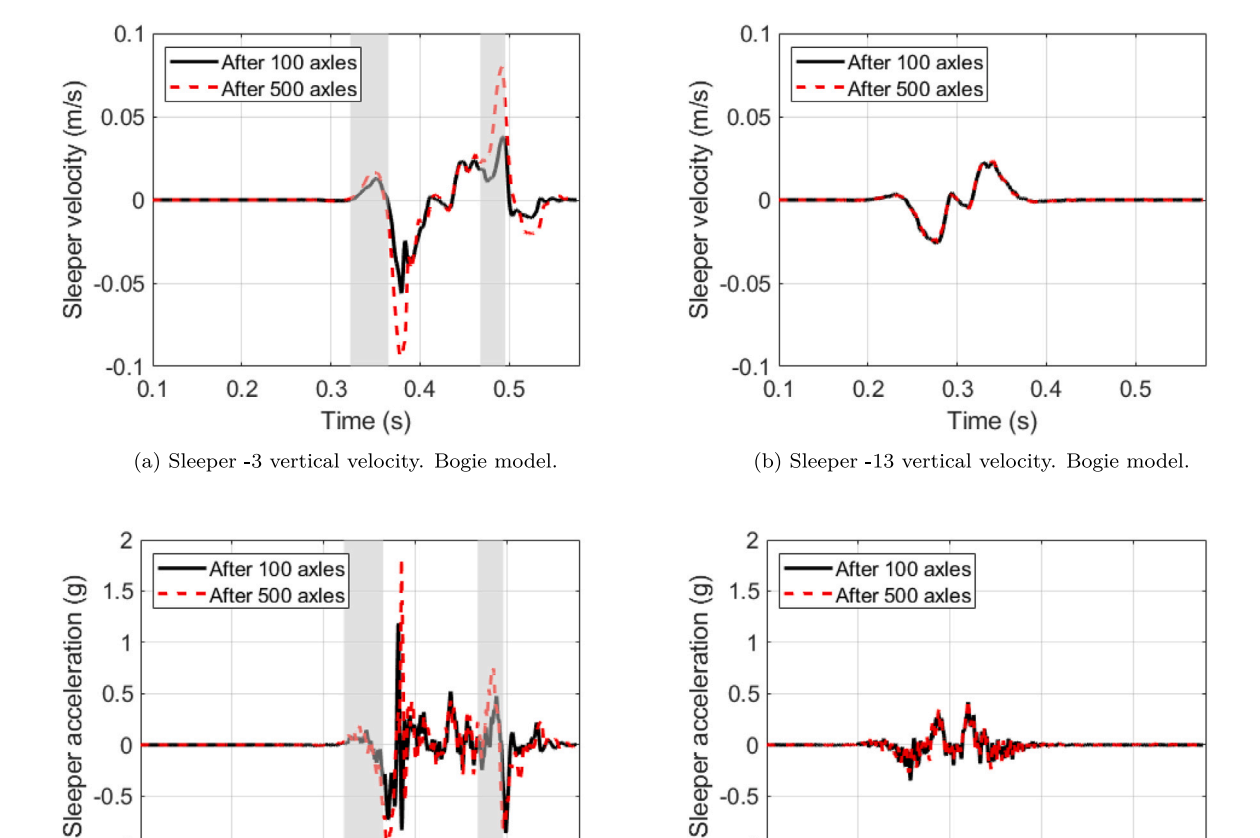


Fig. 17. Time histories of simulated sleeper responses after 100 and 500 axle passages: (a) vertical velocity for sleeper -3; (b) vertical velocity for sleeper -13; (c) vertical acceleration for sleeper -3 is not in contact with the ballast (evaluated after 100 axle passages).

For a traffic load of 10 000 tonnes (500 passes with axle load 20 tonnes), the predicted evolution of accumulated settlement for sleepers -5 and -20 from the transition is shown in Fig. 20. The simulation was performed using the iterative procedure illustrated in Fig. 3 with a sampling interval of 20 axle passes. For each iteration step, and based on the corresponding predicted accumulated settlement, the vertical position of each sleeper on the ballasted side was adjusted in the FEM model before a new set of wheel–rail contact forces was computed as input to the DEM-FDM model. After an initial phase of very rapid settlement development, the rate of permanent displacement slows down. Even though only the initial phase of differential settlement has been considered in this study, the overall trend of long-term settlement seems apparent.

0.2

0.1

0.4

0.5

0.3

Time (s)
(c) Sleeper -3 vertical acceleration. Bogie model.

5. Conclusions

This paper has presented a numerical methodology using a 3D discrete—continuum model coupled with a 2D FEM model to simulate the dynamic performance, and the initial phase of vertical track geometry degradation, in a transition zone between a conventional ballasted track and a stiffer track form. The approach combines the DEM for modelling the granular layers in the ballast and sub-ballast, the FDM for modelling the rail and subgrade, and a FEM model for simulating the dynamic vehicle—track interaction. The granular layers are represented with their appropriate gradation, angular particle shapes, and contact laws, while the continuum model captures the rail structure, sleepers and subgrade layer.

The numerical methodology involves an iterative approach to predict the evolving accumulated differential settlement in the transition zone. For each sleeper, the static support stiffness is determined using the DEM model by applying a static load on the sleeper and simulating the resulting sleeper displacement. These stiffnesses are then used as input data in the FEM model. The subsequently calculated stiffness at rail level reveals a small variation along the ballasted track and a clear stiffness gradient at the transition between the two track forms. The FEM model is coupled with a vehicle MBS model comprising a carbody and two bogies, each supported by two wheelsets, for simulating the time history of wheel-rail contact forces due to dynamic vehicletrack interaction. These calculated wheel-rail contact forces are applied to the DEM-FDM model to predict the differential settlement for all sleepers in the transition zone. In the next iteration step, the settlement of each sleeper is considered in an updated FEM model for a calculation of a new set of wheel-rail contact forces, etc. In this paper, parts of the hybrid DEM-FDM model that had not been validated in previous works have been validated against the calibrated FEM model.

0.2

0.1

0.3

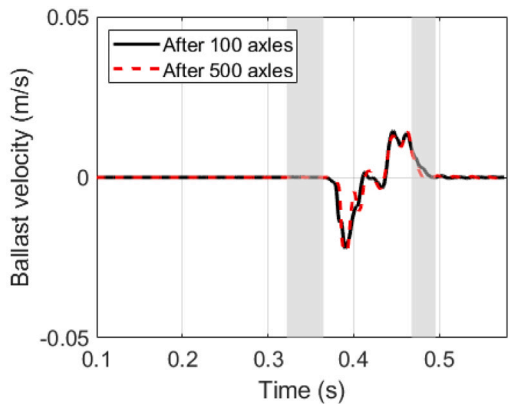
Time (s)

(d) Sleeper -13 vertical acceleration. Bogie model.

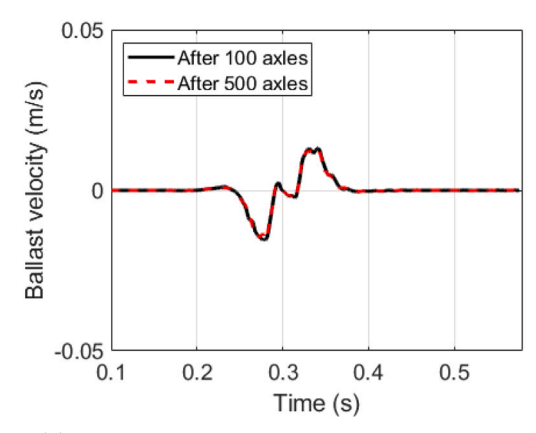
0.4

0.5

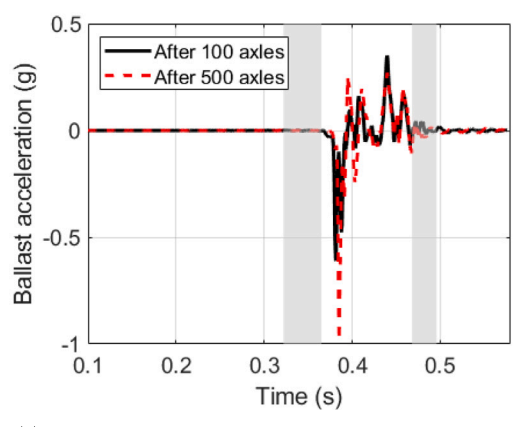
Short-term dynamic responses calculated for rail, sleeper, and ballast indicate higher magnitudes near the transition. Some sleepers in the transition zone are subjected to greater vertical displacements and sleeper–ballast contact forces than the adjacent sleepers. These amplified loads result from the increasing misalignment in rail level due to accumulated differential settlement with increasing number of load cycles (axle passages). As more load cycles are applied, differential settlement increases on the ballasted side. Consequently, some sleepers near the transition become partially suspended from the rail, leading to



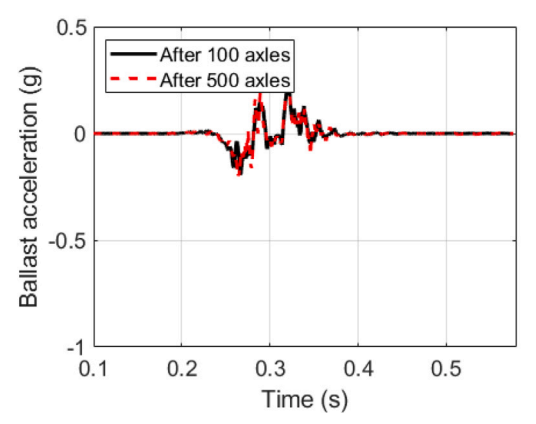
(a) Vertical ballast velocity at sleeper -3. Bogie model.



(b) Vertical ballast velocity at sleeper -13. Bogie model.



(c) Vertical ballast acceleration at sleeper -3. Bogie model.



(d) Vertical ballast acceleration at sleeper -13. Bogie model.

Fig. 18. Time histories of simulated ballast response, at a depth of 20 cm below selected sleepers, after 100 and 500 axle passages, respectively. (a) vertical velocity at sleeper –3; (b) vertical velocity at sleeper –13; (c) vertical acceleration at sleeper –3; (d) vertical acceleration at sleeper –13. The shaded areas show intervals when sleeper -3 is not in contact with the ballast (evaluated after 100 axle passages).

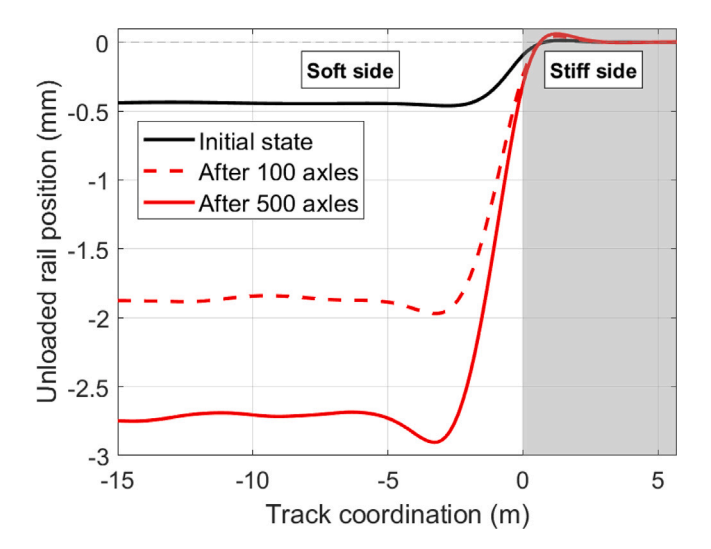


Fig. 19. Predicted rail displacement due to gravity load (no vehicle load) and differential settlement.

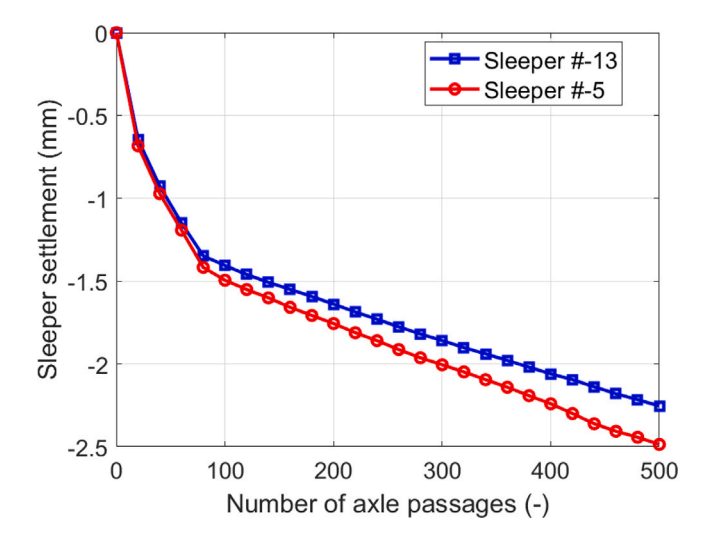


Fig. 20. Predicted sleeper settlement versus number of axle passages. Each iteration step is marked by a symbol.

a redistribution of forces to adjacent sleepers, increasing the magnitude of sleeper–ballast contact forces and more differential settlement for these sleepers.

This behaviour is attributed to the large stiffness gradient at the transition, which leads to higher dynamic loads, particularly due to

the induced low-frequency pitching motion of passing vehicles. Consequently, a local maximum in differential settlement appears on the ballasted side a few metres from the transition. The progressive nature of differential settlement underscores the critical need for a targeted track design and mitigation measures in transition zones.

By illustrating how track geometry and support conditions degrade with cyclic loading, the presented model provides a framework for evaluating track design improvements, such as the implementation of under sleeper pads, transition wedges, wider sleepers, or varying sleeper spacing. In future work, incorporating an advanced ballast degradation model (e.g., to capture fracture or abrasion) could further enhance the accuracy of the long-term settlement prediction. Moreover, the model needs further calibration against experimental data to ensure reliability and applicability.

CRediT authorship contribution statement

Alireza Ahmadi: Writing – review & editing, Writing – original draft, Visualization, Validation, Software, Methodology, Investigation, Formal analysis, Data curation, Conceptualization. Kourosh Nasrollahi: Writing – review & editing, Writing – original draft, Visualization, Validation, Software, Methodology, Investigation, Formal analysis, Data curation, Conceptualization. Jens C.O. Nielsen: Writing – review & editing, Supervision, Resources, Project administration, Methodology, Funding acquisition. Jelke Dijkstra: Writing – review & editing, Supervision, Conceptualization.

Declaration of Generative AI and AI-assisted technologies in the writing process

During the preparation of this work, the authors used ChatGPT in order to improve the coherency and language of the text. After using this tool, the authors reviewed and edited the content as needed and take full responsibility for the content of the publication.

Declaration of competing interest

The authors declare the following financial interests/personal relationships which may be considered as potential competing interests: Alireza Ahmadi reports financial support was provided by Swedish Transport Administration. If there are other authors, they declare that they have no known competing financial interests or personal relationships that could have appeared to influence the work reported in this paper.

Acknowledgements

The authors gratefully acknowledge the Swedish Transport Administration (Trafikverket) for their financial support of this research. The current study is part of the ongoing activities in CHARMEC, Chalmers Railway Mechanics (www.chalmers.se/charmec). Parts of the study have been funded by the Europe's Rail Flagship Project IAM4RAIL – Holistic under grant agreement 101101966. Parts of the computations were enabled by resources provided by Chalmers e-Commons at Chalmers. The authors wish to express their gratitude to Professor Stefan Larsson, Dr. Carl Wersäll, and Professor Magnus Ekh for their valuable feedback on this study.

Data availability

Data will be made available on request.

References

- Aela, P., Powrie, W., Harkness, J., Jing, G., 2024. Discrete element modelling of railway ballast problems: an overview. Arch. Comput. Methods Eng. 1–37.
- Aggestam, E., Nielsen, J.C.O., 2019. Multi-objective optimisation of transition zones between slab track and ballasted track using a genetic algorithm. J. Sound Vib. 446, 91–112.
- Ahmadi, A., 2023. Discrete Element Technique for Modeling High-Speed Railway Tracks (Thesis for the degree of Licentiate in Civil and Architectural Engineering). KTH Royal Institute of Technology, Stockholm, Sweden.
- Ahmadi, A., Larsson, S., 2025. Influence of train travel direction on bridge-embankment transition zones in high-speed railway ballasted tracks. In: Engineering Materials, Structures, Systems and Methods for a more Sustainable Future. CRC Press, pp. 1267–1272.
- Ahmadi, A., Larsson, S., Wersäll, C., 2023. Scaling granular material with polygonal particles in discrete element modeling. Particuology 75, 151–164.
- Ahmadi, A., Wersäll, C., Larsson, S., 2024a. DEM simulation of long railway tracks through utilizing periodic boundaries. In: Applied Numerical Modeling in Geomechanics 2024. Itasca International, Inc., pp. 1–6, Paper No. 12-04.
- Ahmadi, A., Wersäll, C., Larsson, S., 2024b. Impact of particle arrangement and model dimensions on DEM modeling of high-speed railway ballasted tracks in 2D and 3D. Transp. Geotech. 47, 101272.
- Ali, U., Kikumoto, M., Ciantia, M., 2024. Impact of particle elongation on the behavior of round and angular granular media: Consequences of particle rotation and force chain development. Comput. Geotech. 165, 105858.
- Azéma, E., Radjai, F., Saussine, G., 2009. Quasistatic rheology, force transmission and fabric properties of a packing of irregular polyhedral particles. Mech. Mater. 41 (6), 729–741.
- Bian, X., Li, W., Qian, Y., Tutumluer, E., 2020. Analysing the effect of principal stress rotation on railway track settlement by discrete element method. Géotechnique 70 (9) 803–821
- Chen, X., Deng, Y., Chen, N., Deng, Y., 2024. Dynamic characteristics of the sleeper-ballast bed under heavy haul railway train load. Comput. Part. Mech. 11 (3), 1345–1356.
- Chen, J., Vinod, J.S., Indraratna, B., Ngo, T., Liu, Y., 2023. DEM study on the dynamic responses of a ballasted track under moving loading. Comput. Geotech. 153, 105105.
- Chen, C., Zhang, C.-l., Tai, P., Zhang, L., Rui, R., 2025. Optimization of transition section treatments between bridge and regular track using DEM coupled simulation. Transp. Geotech. 101588.
- Christoffersen, J., Mehrabadi, M.M., Nemat-Nasser, S., 1981. A micromechanical description of granular material behavior. J. Appl. Mech. 48 (2), 339–344.
- Chumyen, P., Connolly, D., Woodward, P., Markine, V., 2023. A comparison of earthwork designs for railway transition zones. Constr. Build. Mater. 395, 132295.
- Ciantia, M.O., Boschi, K., Shire, T., Emam, S., 2018. Numerical techniques for fast generation of large discrete-element models. J. Eng. Comput. Mech. 171 (4), 147, 161
- Cui, X., Zhou, R., Guo, G., Du, B., Liu, H., 2021. Effects of differential subgrade settlement on slab track deformation based on a DEM-FDM coupled approach. Appl. Sci. 11 (4), 1384.
- Cundall, P.A., Strack, O.D.L., 1979. A discrete numerical model for granular assemblies. Géotechnique 29 (1), 47–65.
- Dahlberg, T., 2001. Some railroad settlement models A critical review. Proc. Inst. Mech. Eng. Part F: J. Rail Rapid Transit 215, 289–300.
- De Bono, J., McDowell, G., 2020. The effects of particle shape on the yielding behaviour of crushable sand. Soils Found. 60 (2), 520–532.
- de Oliveira Barbosa, J.M., Fărăgău, A.B., van Dalen, K.N., Steenbergen, M.J.M.M., 2022.
 Modelling ballast via a non-linear lattice to assess its compaction behaviour at railway transition zones. J. Sound Vib. 530, 116942.
- Dorador, L., Villalobos, F.A., 2020. Scalping techniques in geomechanical characterization of coarse granular materials. Obras Y Proy. 28, 24–34.
- Eliáš, J., 2014. Simulation of railway ballast using crushable polyhedral particles. Powder Technol. 264, 458–465.
- Fang, J., Zhao, C., Lu, X., Xiong, W., Shi, C., 2023. Dynamic behavior of railway Vehicle-Ballasted track system with unsupported sleepers based on the hybrid DEM-MBD method. Constr. Build. Mater. 394, 132091.
- Fărăgău, A., Jain, A., de Oliveira Barbosa, J., Metrikine, A.V., van Dalen, K.N., 2023. Auxiliary rails as a mitigation measure for degradation in transition zones. In: Proceedings of the Fifth International Conference on Railway Technology: Research, Development and Maintenance, vol. 300. Civil-Comp Press, pp. 1–10.
- Fărăgău, A.B., Metrikine, A.V., van Dalen, K.N., 2019. Transition radiation in a piecewise-linear and infinite one-dimensional structure – a Laplace transform method. Nonlinear Dynam. 98 (4), 2435–2461.
- Fu, L., Tian, Z., Zhou, S., Zheng, Y., Wang, B., 2020. Characterization of ballast particle's movement associated with loading cycle, magnitude and frequency using SmartRock sensors. Granul. Matter 22, 1–13.
- Fu, L., Zheng, Y., Tian, Z., Huang, S., Zhou, S., 2022. Importance of examining particle movements in modelling ballast bed via discrete element method. Int. J. Rail Transp. 10 (5), 547–561.

- Fu, L., Zhou, S., Guo, P., Tian, Z., Zheng, Y., 2021. Dynamic characteristics of multiscale longitudinal stress and particle rotation in ballast track under vertical cyclic loads. Acta Geotech. 16, 1527–1545.
- Guo, Y., Zhai, W., 2018. Long-term prediction of track geometry degradation in high-speed vehicle-ballastless track system due to differential subgrade settlement. Soil Dyn. Earthq. Eng. 113, 1–11.
- Guo, N., Zhao, J., 2014. A coupled FEM/DEM approach for hierarchical multiscale modelling of granular media. Internat. J. Numer. Methods Engrg. 99 (11), 789–818.
- Guo, Y., Zhao, C., Markine, V., Jing, G., Zhai, W., 2020. Calibration for discrete element modelling of railway ballast: A review. Transp. Geotech. 23, 100341.
- Heydari, H., 2023. Evaluating the dynamic behavior of railway-bridge transition zone: numerical and field measurements. Can. J. Civ. Eng. 51 (4), 399–408.
- Indraratna, B., Ngo, T., 2018. Ballast Railroad Design: SMART-UOW Approach. CRC Press.
- Indraratna, B., Ngo, N.T., Rujikiatkamjorn, C., 2011. Behavior of geogrid-reinforced ballast under various levels of fouling. Geotext. Geomembranes 29 (3), 313–322.
- Indraratna, B., Sajjad, M.B., Ngo, T., Correia, A.G., Kelly, R., 2019. Improved performance of ballasted tracks at transition zones: A review of experimental and modelling approaches. Transp. Geotech. 21, 100260.
- Jain, A., Metrikine, A.V., Steenbergen, M.J.M.M., van Dalen, K.N., 2025. Railway transition zones: Energy evaluation of a novel transition structure for critical loading conditions. J. Vib. Eng. Technol. 13 (15).
- Jia, M., Yang, Y., Liu, B., Wu, S., 2018. PFC/FLAC coupled simulation of dynamic compaction in granular soils. Granul. Matter 20 (4), 76.
- Liu, S., Huang, H., Qiu, T., Gao, L., 2017a. Comparison of laboratory testing using smartrock and discrete element modeling of ballast particle movement. J. Mater. Civ. Eng. 29 (3), D6016001.
- Liu, S., Huang, H., Qiu, T., Kwon, J., 2017b. Comparative evaluation of particle movement in a ballast track structure stabilized with biaxial and multiaxial geogrids. Transp. Res. Rec. 2607 (1), 15–23.
- Lommen, S., Mohajeri, M., Lodewijks, G., Schott, D., 2019. DEM particle upscaling for large-scale bulk handling equipment and material interaction. Powder Technol. 352, 273–282.
- Lu, M., McDowell, G., 2007. The importance of modelling ballast particle shape in the discrete element method. Granul. Matter 9 (1), 69–80.
- Luo, Z., Zhao, C., Bian, X., Chen, Y., 2023. Discrete element analysis of geogridstabilized ballasted tracks under high-speed train moving loads. Comput. Geotech. 159, 105451.
- Milosevic, M.D.G., Pålsson, B.A., Nissen, A., Nielsen, J.C.O., Johansson, H., 2023. Reconstruction of sleeper displacements from measured accelerations for model-based condition monitoring of railway crossing panels. Mech. Syst. Signal Process. 192, 110225.
- Nabochenko, O., Sysyn, M., Fischer, S., 2024. Ballast settlement accumulation in zones with unsupported sleepers. Transp. Infrastruct. Geotechnol. 11 (4), 2598–2637.
- Nakamura, H., Takimoto, H., Kishida, N., Ohsaki, S., Watano, S., 2020. Coarse-grained discrete element method for granular shear flow. Chem. Eng. J. Adv. 4, 100050.
- Nasrollahi, K., 2025. Transition Zone Design for Reduced Track Settlements: Field Measurements and Numerical Simulations (Phd thesis). Chalmers University of Technology, Gothenburg, Sweden.
- Nasrollahi, K., Dijkstra, J., Nielsen, J.C.O., 2024a. Towards real-time condition monitoring of a transition zone in a railway structure using fibre Bragg grating sensors. Transp. Geotech. 44, 101166.
- Nasrollahi, K., Nielsen, J.C.O., 2024. Influence of sleeper base area and spacing on long-term differential settlement in a railway track transition zone. In: Proceedings of the Sixth International Conference on Railway Technology: Research, Development and Maintenance. Civil-Comp Conferences', pp. 1–11.
- Nasrollahi, K., Nielsen, J.C.O., Aggestam, E., Dijkstra, J., Ekh, M., 2023. Prediction of long-term differential track settlement in a transition zone using an iterative approach. Eng. Struct. 283, 115830.
- Nasrollahi, K., Ramos, A., Nielsen, J.C.O., Dijkstra, J., Ekh, M., 2024b. Benchmark of calibrated 2D and 3D track models for simulation of differential settlement in a transition zone using field measurement data. Eng. Struct. 316, 118555.
- Ngamkhanong, C., Feng, B., Tutumluer, E., Hashash, Y.M.A., Kaewunruen, S., 2021. Evaluation of lateral stability of railway tracks due to ballast degradation. Constr. Build. Mater. 278, 122342.
- Nie, Z., Fang, C., Gong, J., Liang, Z., 2020. DEM study on the effect of roundness on the shear behaviour of granular materials. Comput. Geotech. 121, 103457.
- Nielsen, J.C.O., 2008. High-frequency vertical wheel-rail contact forces Validation of a prediction model by field testing. Wear 265 (9–10), 1465–1471.
- Nielsen, J.C.O., Li, X., 2018. Railway track geometry degradation due to differential settlement of ballast/subgrade Numerical prediction by an iterative procedure. J. Sound Vib. 412, 441–456.
- Ognibene, G., 2023. Relating Trackbed Stiffness and Behaviour with Track Performance and Maintenance Needs (Ph.D. thesis). School of Engineering, University of Southampton, United Kingdom, p. 262.
- O'Sullivan, C., 2011. Particulate Discrete Element Modelling: A Geomechanics Perspective. CRC Press.
- Paixão, A., Fortunato, E., Calçada, R., 2014. Transition zones to railway bridges: track measurements and numerical modelling. Eng. Struct. 80.

- Punetha, P., Nimbalkar, S., 2023. Numerical investigation on dynamic behaviour of critical zones in railway tracks under moving train loads. Transp. Geotech. 41, 101009
- Radjai, F., Dubois, F., 2011. Discrete-Element Modeling of Granular Materials. Wiley-ISTE, 425 pages.
- Ramos, A., Correia, A.G., Nasrollahi, K., Nielsen, J.C.O., Calçada, R., 2024. Machine learning models for predicting permanent deformation in railway tracks. Transp. Geotech. 47, 101289.
- Ramos, A., Gomes Correia, A., Calçada, R., Connolly, D.P., 2022. Ballastless railway track transition zones: An embankment to tunnel analysis. Transp. Geotech. 100728.
- Sañudo, R., Dell'Olio, L., Casado, J., Carrascal, I., Diego, S., 2016. Track transitions in railways: A review. Constr. Build. Mater. 112, 140–157.
- Saussine, G., Cholet, C., Gautier, P., Dubois, F., Bohatier, C., Moreau, J.-J., 2006. Modelling ballast behaviour under dynamic loading. Part 1: A 2D polygonal discrete element method approach. Comput. Methods Appl. Mech. Engrg. 195 (19–22), 2841–2859.
- Selig, E.T., Waters, J.M., 1994. Track Geotechnology and Substructure Management. Thomas Telford.
- Seyyedan, S.M., Mirghasemi, A.A., Mohammadi, S., 2021. Numerical simulation of direct shear test on granular materials composed of breakable angular particles: A DEM-XFEM approach. Powder Technol. 391, 450–466.
- Shan, Y., Zhou, S., Wang, B., Ho, C.L., 2020. Differential settlement prediction of ballasted tracks in bridge-embankment transition zones. J. Geotech. Geoenviron. Eng. 146 (9), 04020075.
- Shao, X., Yang, Z., Jiang, Y., Feng, J., 2022. Coupled FDM-DEM method for analyzing EPBS machine tunneling performance in boulders. Int. J. Geomech. 22 (12), 04022239.
- Shi, C., Chen, Z., 2021. Coupled DEM/FDM to evaluate track transition stiffness under different countermeasures. Constr. Build. Mater. 266, 121167.
- Shi, C., Zhao, C., Xin, L., Wang, J., 2024. Dynamic impact of unsupported sleepers on railway infrastructure with a coupled MBD-DEM-FDM model. Transp. Geotech. 45, 101221.
- Shi, C., Zhao, C., Zhang, X., Guo, Y., 2021. Coupled discrete-continuum approach for railway ballast track and subgrade macro-meso analysis. Int. J. Pavement Eng. 22 (13), 1744–1759.
- Siahkouhi, M., Rashidi, M., Miri, A., Ghiasi, A., Paixão, A., 2025. Ballasted railway track-bridge transition zone monitoring methods: Recent developments, challenges, and prospects. J. Transp. Eng. Part B: Pavements 151 (3), 03125001.
- Smeets, B., Odenthal, T., Vanmaercke, S., Ramon, H., 2015. Polygon-based contact description for modeling arbitrary polyhedra in the discrete element method. Comput. Methods Appl. Mech. Engrg. 290, 277–289.
- Stastny, A., Emera, A., Galavi, V., Tschuchnigg, F., 2025. Cyclic soil-structure interaction of integral railway bridges. Front. Built Environ. 11, 1541282.
- Suhr, B., Six, K., 2020. Simple particle shapes for DEM simulations of railway ballast: influence of shape descriptors on packing behaviour. Granul. Matter 22 (2). 43.
- Suhr, B., Skipper, W.A., Lewis, R., Six, K., 2022. DEM modelling of railway ballast using the Conical Damage Model: A comprehensive parametrisation strategy. Granul. Matter 24 (1), 1–25.
- Suiker, A., de Borst, R., 2003. A numerical model for the cyclic deterioration of railway tracks. Internat. J. Numer. Methods Engrg. 57, 441–470.
- Sun, Q., Indraratna, B., Nimbalkar, S., 2014. Effect of cyclic loading frequency on the permanent deformation and degradation of railway ballast. Géotechnique 64, 746–751.
- Talebi, N., Ahlström, J., Ekh, M., Meyer, K.A., 2024. Evaluations and enhancements of fatigue crack initiation criteria for steels subjected to large shear deformations. Int. J. Fatigue 182, 108227.
- Tan, P., Xiao, Y., Jiang, Y., Wang, M., Wang, X., Zhang, C., Tutumluer, E., 2024. Investigating influencing mechanisms of under-sleeper pads on lateral resistance of ballasted railway trackbed via hybrid DEM-FDM simulations. Transp. Geotech. 45, 101200.
- Tizpa, P., Chenari, R.J., Payan, M., 2023. PFC/FLAC 3D coupled numerical modeling of shallow foundations seated on reinforced granular fill overlying clay with square void. Comput. Geotech. 161, 105574.
- Unsiwilai, S., Shen, C., Zeng, Y., Wang, L., Núñez, A., Li, Z., 2024. Vertical dynamic measurements of a railway transition zone: A case study in Sweden. J. Civ. Struct. Heal. Monit. 14 (4), 979–996.
- Vizcarra, G.C., Nimbalkar, S., Casagrande, M., 2016. Modeling behaviour of railway ballast in prismoidal apparatus using discrete element method. Procedia Eng. 143, 1177–1184.
- Wang, H., Markine, V., 2018. Modelling of the long-term behaviour of transition zones: Prediction of track settlement. Eng. Struct. 156, 294–304.
- Wang, Y., Mora, P., Liang, Y., 2022. Calibration of discrete element modeling: Scaling laws and dimensionless analysis. Particuology 62, 55–62.
- Xiao, J., Xue, L., Zhang, D., Sun, S., Bai, Y., Shi, J., 2023. Coupled DEM-FEM methods for analyzing contact stress between railway ballast and subgrade considering real particle shape characteristic. Comput. Geotech. 155, 105192.
- Yousefi, A., Ng, T.-T., 2017. Dimensionless input parameters in discrete element modeling and assessment of scaling techniques. Comput. Geotech. 88, 164–173.
- Zhang, X., Zhao, C., Zhai, W., 2019. Importance of load frequency in applying cyclic loads to investigate ballast deformation under high-speed train loads. Soil Dyn. Earthq. Eng. 120, 28–38.
- Zuada Coelho, B., Dijkstra, J., Karstunen, M., 2021. Viscoplastic cyclic degradation model for soft natural soils. Comput. Geotech. 135, 104176.
- model for soft natural soils. Comput. Geotech. 135, 104176.
 Zuada Coelho, B., Hölscher, P., Priest, J., Powrie, W., Barends, F., 2011. An assessment of transition zone performance. Proc. Inst. Mech. Eng. Part F: J. Rail Rapid Transit 225 (2), 129–139.